

Preparation and characterization of p-n homojunction Cu_2O nanowire solar cells

Bachelor's Thesis R. H. A. Cornelissen

July 12, 2012

Graduation committee:

Chairperson: Prof. Dr. Ir. J. E. ten Elshof

Daily supervisor: A. W. Maijenburg, Msc.

External examiner: Dr. H. K. Hemmes

Member: Dr. Ir. M. Huijben

Inorganic Materials Science
Faculty of Science and Technology
University of Twente

Abstract

This thesis presents an experimental study on the preparation and characterisation of p-n homojunction Cu₂O nanowire solar cells. The investigated preparation route starts with templated electrodeposition of p-type Cu₂O nanowires. After dissolution of the template, free standing nanowires are left. Then a bottom layer of p-type Cu₂O is deposited and a final electrodeposition of n-type Cu₂O fills the voids and forms the p-n junction. Nanowires were successfully deposited, however dissolution of the membrane was not successful; a 40nm residual layer was left, which resulted in the impossibility to deposit the bottom p-type layer. Without the bottom deposition, it was tried to create a p-n junction by directly depositing the n-type Cu₂O on top of the nanowires. Characterisation was carried out by a chrono amperometric measurement of the nanowires in NaSO₄ and linear sweep voltage measurements on the synthesised solar cells. The nanowires showed a relatively high photocurrent density of 47 $\mu\text{A}/\text{cm}^2$. Most of the solar cells provided linear I-V curves, probably due to internal short circuit. Although two of the solar cells showed p-n junction like behaviour, no photocurrent was generated.

Table of contents

1	Introduction	1
2	Theoretical background.....	2
2.1	Solar cells.....	2
2.1.1	Semiconductors.....	2
2.1.2	Photovoltaic effect.....	4
2.1.3	Characterisation.....	5
2.1.4	Solar cell design.....	7
2.2	Cuprous Oxide (Cu ₂ O).....	11
2.2.1	p-type.....	11
2.2.2	n-type.....	12
2.3	Nanostructure synthesis.....	13
2.3.1	Template types.....	13
2.3.2	Templated electrodeposition of Cu ₂ O.....	14
2.3.3	Template free electrodeposition of Cu ₂ O.....	15
3	Experimental details.....	17
3.1	Chemicals used.....	17
3.2	p-n homojunction solar cell preparation.....	17
3.2.1	Sample preparation (A+B).....	17
3.2.2	Nanowire deposition (C).....	18
3.2.3	Template dissolution (D).....	18
3.2.4	Bottom deposition (E).....	19
3.2.5	Void deposition (F).....	19
3.2.6	Top contact deposition (G).....	19
3.3	Sample inspection.....	19
3.4	Sample characterisation.....	20
3.4.1	Nanowires photocurrent measurement.....	20
3.4.2	Solar cell photocurrent measurements.....	21
4	Results and discussion	22
4.1	Preparation process of the p-n homojunction.....	22
4.1.1	Sample preparation.....	22
4.1.2	Nanowire electrodeposition.....	23
4.1.3	Template dissolution.....	25
4.1.4	Bottom layer deposition.....	28
4.1.5	n-type deposition.....	30
4.2	Sample characterisation.....	32
4.2.1	Nanowire photocurrent.....	32

4.2.2	Solar cell photocurrent.....	35
5	Conclusions.....	38
5.1	Preparation.....	38
5.2	Characterization	39
6	Recommendations	40
	Acknowledgements	41
	References.....	43

1 Introduction

Society is dealing with an ever increasing energy demand; while the current energy source, fossil fuels, will be depleted in the near future, since the 80's each year more fossil fuels are consumed than new reserves found. A new energy source is thus needed; many different fields are currently investigated to find renewable energy sources to replace the fossil fuels. One of these fields is solar power, which is a promising power source since the radiation power of the sun that reaches the earth is ~2850 times the current energy demand of the planet [1]. Even harvesting just a small amount of this energy delivers a great source of energy.

Currently, the solar energy market is dominated by crystalline silicon solar cell modules, since they have a relatively high efficiency, quite low prices and a long life time. Nevertheless, solar power encompasses only a small portion of our total energy sources. For a broader adaption of solar energy, the price of solar energy needs to drop even more. This can be accomplished by either increasing the efficiency or by reducing the production costs.

The use of nanowires is one of the innovations that looks promising for reaching this goal; the charge separation is faster resulting in a higher efficiency. Furthermore they can be made from all kinds of materials, so also cheaper and more abundant materials than the ones currently used in solar cells. Cuprous oxide is a material that seems promising for making nanowire solar cells. Cuprous oxide has some advantages over the currently used materials: it is abundant, is relatively cheap, has a suitable band gap, is non toxic and has a good absorption coefficient. The disadvantage of the material is that its theoretically efficiency is only 12% [2]. Progress has been made in making Cu_2O p-n homojunction multilayer solar cells, which have reached an efficiency of 1.06% [3]. With the use of nanowires a greater interface can be created and is thus expected to increase the efficiency.

During the last couple of years, procedures for the synthesis of electrochemically synthesised nanowires have been developed in the Inorganic Materials Science lab (IMS) at the University of Twente [4-8]. By this method, templated electrodeposition, billions of free-standing metal-oxide nanowires can be created.

Templated electrodeposition can be used to create free standing p- Cu_2O nanowires. By filling the voids between the wires with n- Cu_2O , a p-n homojunction Cu_2O solar cell with a much larger interface is created. This larger interface is likely to increase the efficiency compared to multilayered solar cells, since the charges have a higher chance of being separated.

In this thesis research is done on these nanowire solar cells, by finding a way of preparing these solar cells and characterising their behaviour. The first goal of the research is to find a preparation route to synthesize p-n homojunction Cu_2O nanowire solar cells. The second goal is to characterise these solar cells, and thus comparing their efficiency to the current p-n Cu_2O homojunction multilayer solar cells.

2 Theoretical background

2.1 Solar cells

A solar cell is an electronic device that directly converts sunlight into electricity, opposite to solar heat installations in which sun light is used to form steam and operate an ordinary steam turbine [9]. An illuminated solar cell produces a current as well as a voltage which can be harvested by an external circuit or power an integrated circuit, i.e. calculators. For this effect, semiconductors are necessary, which are materials with special electronic properties. The current state of our technology wouldn't be possible without these materials.

2.1.1 Semiconductors

Materials can be classified in three categories of conduction: conductors, semiconductors and insulators. These classifications come from the electrical properties of the material, which are determined by its energy levels. It is important to know that due to quantum mechanics, in an atom only certain discrete electron energy levels are allowed. From this theory also follows the Pauli exclusion principle which says that two electrons with the same spin cannot occupy the same energy level. In bulk material the energy levels spread into energy bands consisting of discrete energy levels. Those energy bands are either separated from each other or overlapping depending on the separation distance between the atoms (Figure 1) [10]. If the energy bands are separated an energy gap between the two bands exists, which is called the band gap (E_g). The energy bands are divided in three categories:

1. The valence band; the highest at least partially filled energy band
2. The core bands; all the energy bands below the valence band
3. The conduction band; the empty energy band above the valence band

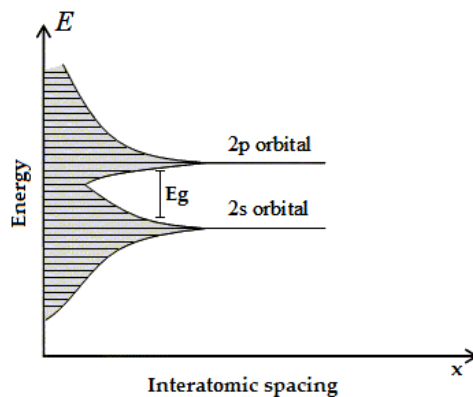


Figure 1: The energy band diagram as a function of the interatomic spacing, with E_g as the band gap.

For electrical conduction to be possible, the presence of empty energy levels that are not too far apart from levels occupied by electrons is necessary. The reason for this is that if an electron moves, it has a slightly higher energy than when it is not moving, so to be able to move it needs to occupy a higher energy level. If an energy band is just sparsely filled with electrons, the conduction is equal to the amount of electrons; each electron can occupy a higher energy level. Although, when the energy band gets filled up with more electrons it is possible for less electrons to move, until it is completely filled and no conduction can take place. In case of just a few empty energy states in the energy band the conduction can take place by 'holes', which are free energy levels in a nearly filled energy band. This is due to the fact that if an electron moves to the hole, the hole moves in the opposite direction, if now another electron moves to the hole, the hole moves even further. This movement of electrons and holes can either be viewed as the motion of two electrons or as one hole moving two energy levels. Thus the hole can be viewed as a charge carrier equal in magnitude but opposite in sign to that of an electron. [10]

Looking at the classification of the materials by electrical conductivity, it is clear that a conductor, since it can conduct, will have a valence band that is partially filled. The semiconductor and the insulator both have completely filled valence bands; however the semiconductor distinguishes itself from the insulator since it has a smaller band gap. Arbitrarily a material is seen as a semiconductor when its band gap is smaller than 2.5 eV [10], for intrinsic semiconductors. This band gap is sufficiently small that by adding only a small amount of energy, i.e. by heat, electrons are promoted to the conduction band and thus the conductivity of the material increases. [10, 11]

Semiconductors are divided into two categories: intrinsic and extrinsic semiconductors. Intrinsic conduction is defined as semiconducting behaviour resulting from the structure of a pure element. In contrast, extrinsic conduction originates from the presence of dopants or impurities, for which the previous mentioned arbitrary border of a band gap of 2.5 eV does not count. Since electrons are promoted to the acceptor level or from the donor level, instead of over the entire band gap. [10-13]

For an extrinsic semiconductor, it is possible to exhibit semiconducting behaviour, due to the electrons of the dopant or impurity. These electrons are not restricted to the energy levels of the bulk material, i.e. they actually can exist in the band gap of the bulk material (Figure 2). This phenomenon is the basis for extrinsic conduction. [10-13]

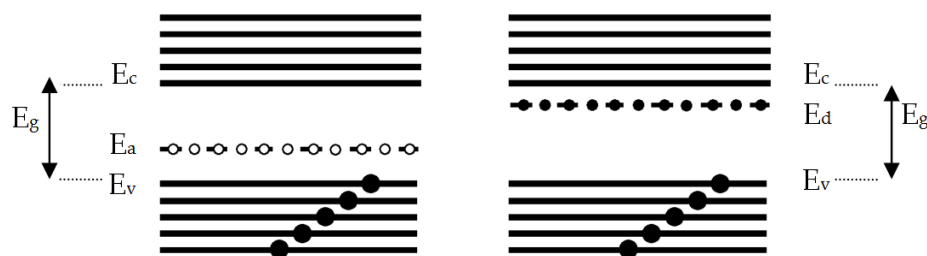


Figure 2: Energy band diagram of p-type (left) and n-type (right) semiconductors. E_c is the conduction energy level, E_a is the donor energy level, E_v is the valence energy, E_d is the acceptor energy and E_g is the band gap energy.

Consider silicon doped with a small amount of arsenic. Since arsenic has five electrons in its valence band and silicon only four, there is an extra electron. This electron is only weakly bound and occupies an energy level just below the conduction band, and so it is easily promoted to the conduction band. Such a semiconductor is called an n-type semiconductor, with the n for negative (Figure 2).

Just as introducing a dopant with more electrons in the valence band than the bulk material, it is also possible to dope the bulk material with an element with less valence electrons. Doping silicon with Gallium is such a semiconductor. Gallium has only three valence electrons, leaving one electron of the silicon unbound, resulting in a "hole". This creates empty energy levels just above the valence band, which can accept electrons and thus leaving behind a hole in the valence band that is free to propagate. Such a semiconductor is called a p-type semiconductor, with the p for positive (Figure 2).

2.1.2 *Photovoltaic effect*

By combining p- and n-type semiconductors, it is possible to make electronic devices such as diodes, transistors, LED's and of course solar cells. The simplest electronic device is probably the p-n junction diode. This diode is made by putting an n-type semiconductor in contact with a p-type semiconductor, creating a region rich of holes and a region rich of electrons. At the interface between the two semiconductors a depletion zone will form due to the recombination of holes and electrons in this region. At this interface, an electric field is present opposite to the gradient of the concentration of charge carriers, due to the fact that the electric field is not generated by the charge carriers but by the atoms that delivered the charge carriers. Due to this electric field, the recombination of charge carriers is not possible in the bulk but only at the interface, and thus limiting the size of the depletion zone. [10-14]

If a potential is applied to a p-n junction diode, connecting a positively charged electrode to the p-type side, the applied potential difference will force the charge carriers (both holes and electrons) to move to the interface, and therefore enhance the recombination of holes and electrons, which results in a current. However, if the potential is reversed, the charge carriers will be attracted to the electrodes instead of the interface, hence no recombination will occur and consequently no current will flow. Essentially the diode is only able to conduct in one direction. These two potentials are called forward and reverse biased respectively. The I-V characteristic of this device is shown in Figure 3. [10-14]

Solar cells are based on the same principle as diodes: a p-n junction. When the device is illuminated, photons will penetrate into the material. If a photon with a higher energy than the band gap penetrates the p-type region, three situations are possible: (1) the photon goes straight through the material, (2) the photon is reflected or (3) the photon is absorbed by an atom. If the photon is absorbed, it will excite an electron from the valence band into the conduction band, leaving a hole in the valence band. [11, 14, 15]

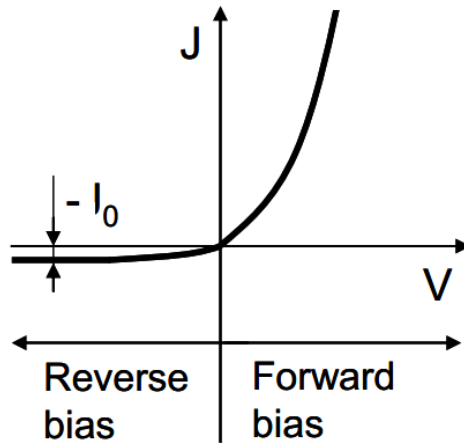


Figure 3: I-V characteristic of an ideal p-n diode.

A p-n junction device has a natural electric field at the interface of p- and n-type material due to the recombination of charges. This electric field causes the generated electrons to be accelerated to the n-type material and the generated holes to the p-type material, if they are not recombined before reaching the n- or p-type region [14]. This process creates an excess of charge at both sides of the device and thus an increased potential. When a resistance (load) is connected to the device a current will flow and thus the lights energy is harvested, by conversion to electrical power. [14, 15]

2.1.3 Characterisation

Since solar cells are actually specially designed p-n junction devices, equations important for characterisation of p-n junctions are likewise important for solar cells. A fundamental equation for microelectronics is the Shockley equation (Eq. 1) which describes the behaviour of an ideal p-n diode. [16]

$$I(V_a) = I_0 \left[\exp\left(\frac{qV_a}{kT}\right) - 1 \right] \quad 1$$

Where the current (**I**) is given as a function of the applied voltage (V_a). This function consists of two physical parts: the recombination current represented by the exponent function and the thermodynamically generated current which is equal to the short circuit current (I_0) and not dependent on the applied voltage. Furthermore, **k** is the Boltzmann constant, **q** the charge of an electron and **T** the temperature. This equation shows the behaviour described for a p-n diode, so current will flow when a forward-biased voltage is applied. However, when a reverse-biased voltage is applied, the exponential becomes small and can be neglected so the current is equal to $-I_0$. [16]

When a solar cell is illuminated, extra charge carriers in the form of electron-hole pairs are formed. These extra charges are separated as electrons move to the n-type material and the holes to the p-type material. The flow of these charge carriers causes a current: the photogenerated current (I_{ph}). In case of an open circuit, no current can flow in the device so this current has to be balanced, which is done by the recombination current. But when the device is in a short circuit, photogenerated

current will also flow through the external circuit. When a load is connected in this short circuit, only a fraction of the photogenerated current will flow through the external circuit. The net current flowing through the circuit depends on the same two currents as in the p-n junction but now also the photogenerated current has to be taken into account, resulting in equation 2. [16]

$$I(V_a) = I_0 \left[\exp\left(\frac{qV_a}{kT}\right) - 1 \right] - I_{ph} \quad 2$$

Under no illumination, equation 2 reduces to the Shockley equation, since the photogenerated current becomes zero, but when illuminated the photogenerated current will decrease the current, resulting in a negative current, and thus delivering power ($I \cdot V$). This behaviour is clearly visible in Figure 4, when the cell is in the dark you have the same I-V relation as for a p-n junction, but when illuminated, the I-V curve is shifted downwards by the photogenerated current. [16]

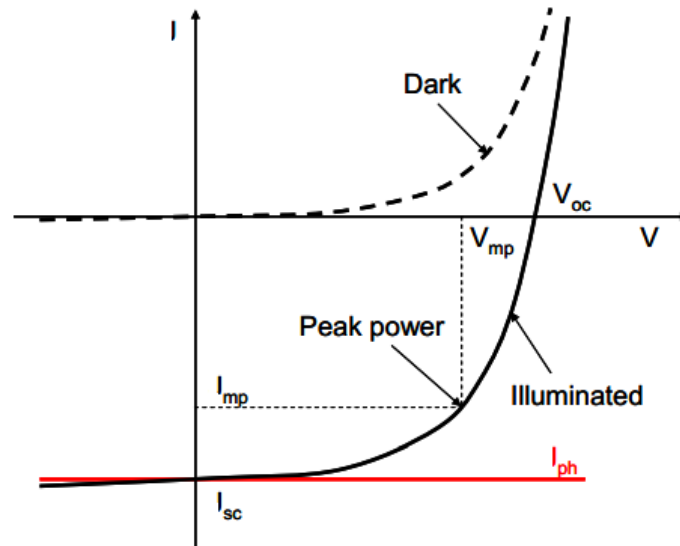


Figure 4: I-V characteristics of an ideal solar cell in the dark and under illumination.

The photogenerated current is the driving force of the solar cell, so improving the photocurrent will greatly increase the efficiency. The photogenerated current is given in equation 3:

$$I_{ph} = qG(L_n + W + L_p)A_i \quad 3$$

were G is the charge carriers generation rate, W is the width of the depletion zone, A_i the area of the interface and L_n and L_p are the diffusion lengths of electrons and holes, respectively. In the equation, it is shown that only carriers generated in the depletion zone and a diffusion length from the depletion zone contribute to the photocurrent. The charge carrier diffusion length is the average length a charge carrier can travel before recombination occurs, thus if this length is larger more charges diffuse into the depletion zone and separated. [15, 16]

Looking at Figure 4, the most important parameters for characterising the performance of solar cells can be found: the short circuit current (I_{sc}), which is the value for the current at no voltage so the intersection with the I-axis. Dividing I_{sc} by the measured solar cell area gives the short circuit current density (J_{sc}). The open circuit voltage (V_{oc}) is the voltage for no current, so the intersection with the V-axis. By multiplying the current and the voltage over the whole graph, a power per voltage graph can be made and from this the maximum power can be extrapolated. The voltage and power for maximum power are V_{mp} and I_{mp} .

The fill factor (**FF**) is an important ratio that can be calculated from these parameters. The fill factor (eq. 4) is the ratio between the maximum power and the product of the open circuit voltage with the short circuit current. The fill factor can be seen as a measurement for the “squareness” of the I-V curve, a higher value for **FF** gives a more squared like shape, resulting in a V_{mp} and I_{mp} getting closer to the I_{sc} and V_{oc} , hence increasing the maximum power output. [15, 16]

$$FF = \frac{I_{mp}V_{mp}}{I_{sc}V_{oc}} \quad 4$$

The conversion efficiency (η), equation 5, is the most important ratio; it is the ratio between the generated power and the incident power. The incident power is the energy in the light source; the standard used in solar cell research is 1000 W/m² of the AM1.5 spectrum. [15, 16]

$$\eta = \frac{P_m}{P_{in}} = \frac{I_{sc}V_{oc}FF}{P_{in}} \quad 5$$

2.1.4 Solar cell design

The most important design aspect of a solar cell is of course its efficiency. Achieving a high efficiency can be achieved by many design parameters i.e. semiconductor material, shape, contact material, glass and crystal structure. A semiconductor material needs to fulfil several criteria to be useful for application in photovoltaic cells. Most of these criteria can be linked to the photocurrent generation as shown in equation 3.

The first criterion is chemical stability, which is important since solar cells are used for many years to be profitable. So in the conditions it is used, it should be reliable for quite some time, without being affected by its environment, i.e. sun light, air and water.

The second criterion, the band gap, influences the generation coefficient (eq. 3) by its influence on the absorbed spectrum. The band gap energy is the minimum energy a photon needs to possess for exciting an electron to a higher energy band, hence creating charge carriers. Since the band gap energy is the minimum photon energy, photons with a higher energy are thus also absorbed. Cuprous oxide for instance has a band gap of 1.9-2.2 eV [17], which corresponds to a wavelength of ~572nm. This means that wavelengths shorter (higher energy) than 572nm can be absorbed. This behaviour is also clearly visible in Figure 5, reproduced from [18], it

shows the absorption coefficient per photon energy. There is a sharp increase in absorption around 2 eV due to the band gap.

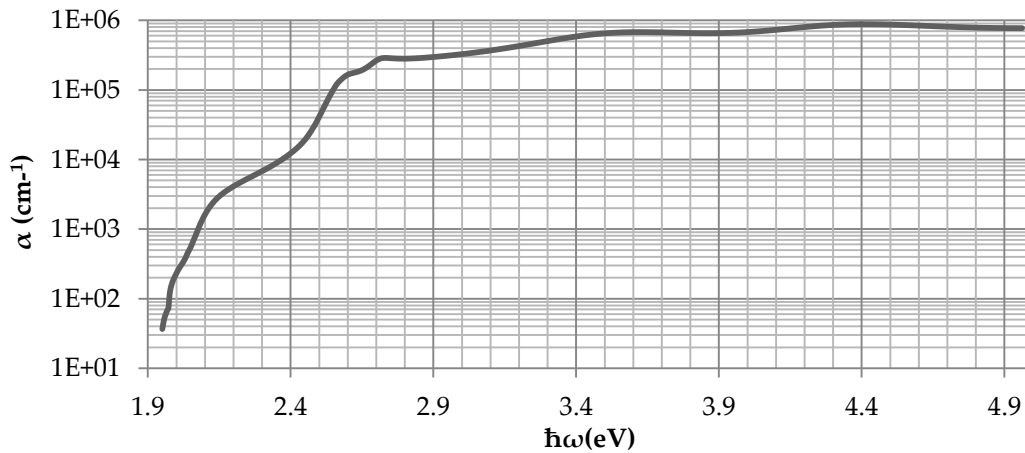


Figure 5: Absorption coefficient of Cu_2O .

The third criterion is this absorption coefficient, which influences the amount of photons absorbed of a certain spectrum. A higher absorption coefficient means that if a photon penetrates the material, the photon has a greater chance of being absorbed instead of being passed through or scattered. Hence, a high absorption coefficient means that a thinner layer of semiconductor is enough to absorb all or a large part of the light, so the maximum amount of charge carriers is generated. The absorption coefficient of Cu_2O is shown in Figure 5, for several photon energies, first a sharp increase due to the band gap at ~ 1.9 eV is seen, after this increase it stays more or less constant, which means that absorbing light at a low photon energy (large wavelength) will be most difficult [18].

From the absorption coefficient, the percentage of absorbed light per photon energy (or wavelength) can be calculated. This is shown in Figure 6 for several thicknesses of a Cu_2O . In this figure, the radiated power per photon energy of the solar spectrum (AM 1.5) is also depicted; the most power is radiated at a photon energy of around 2.5 eV. It is visible that for energies higher than 2.5 eV, the absorbed amount of light is independent of the thickness of the semiconductor as long as it is thicker than 100nm. However, for lower energies it is particularly important; both since the power of the solar light is decreasing at a substantial slower rate for energies below 2.5 eV than above, as well as the rather large difference in percentages absorbed in this energy region.

It is tempting to make the photovoltaic cell very thick to absorb a great percentage over the entire spectrum above the band gap. Although cost and structural strength also have to be accounted for, but even more important: photons absorbed far from the interface do not contribute to the photocurrent, as is shown in the photocurrent equation (eq. 3). The carriers generated further away from the interface than the charge diffusion length are not separated and thus do not contribute to the photocurrent.

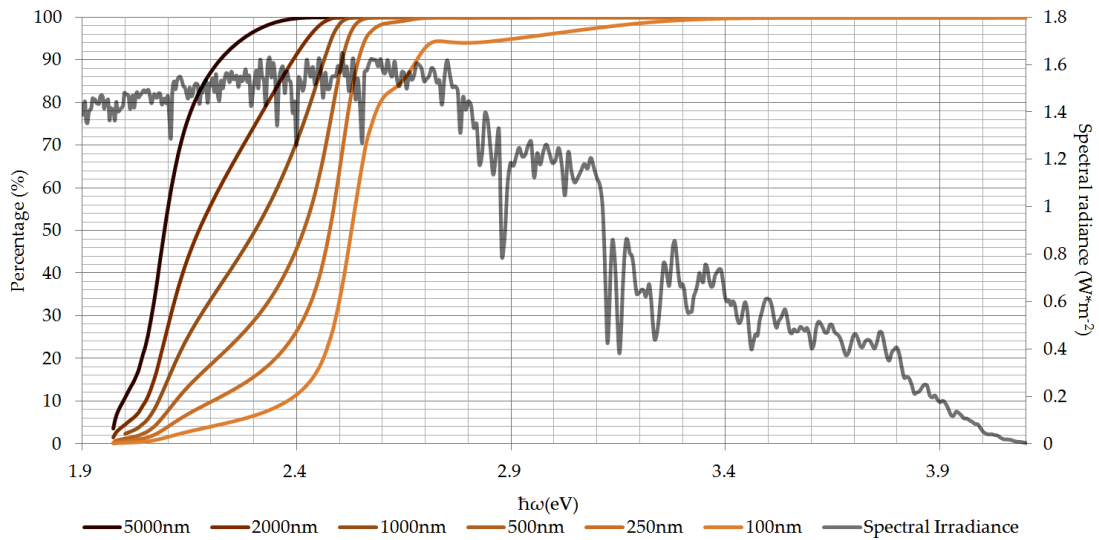


Figure 6: Percentage absorbed vs. photon energy for several thicknesses and the spectral irradiance of the solar spectrum (AM1.5 Global spectrum, ASTM G173).

This charge carrier diffusion is the fourth criterion. The charge carrier diffusion length is the average length a charge carrier will travel before recombination occurs. This is important since charge is only separated in the depletion zone, i.e. if the charge carriers have a high diffusion length, more charge diffuses into the depletion zone and thus separated. In Cu_2O charge carriers have a rather large diffusion length of 10-100nm [19], hence material more than 100nm away from the depletion zone has no contribution to the photocurrent.

The last criterion for a semiconductor material to be suitable for solar cell application is low cost and abundance. Since (most) solar cells will be used for mass power production the price should be low enough to compete with other renewable energy sources and even fossil fuels with its increasing costs.

Besides, the semiconductor material choices have to be made in the form factor of the solar cell. The simplest way to create the p-n junction is by means of a multilayer: just a p- and n-type layer on top of each other [2, 3, 20-22]. However, this method gives the smallest junction area; this junction area can be increased by synthesising different shapes of p-n junctions, as shown in Figure 7 [19].

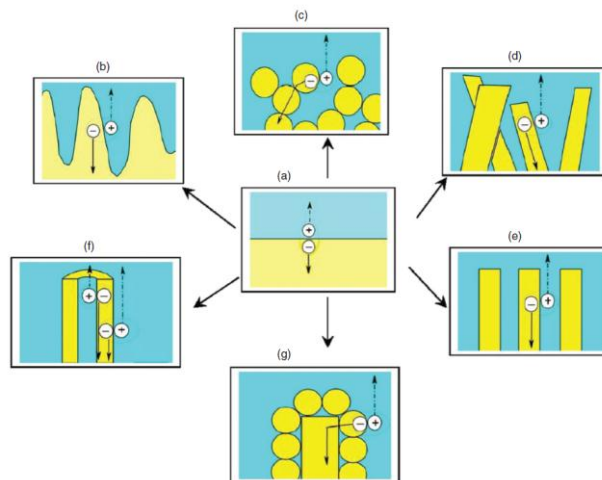


Figure 7: Several p-n junction designs for increasing interface between the p- and n-type material.

A possibility for increasing the interface surface is by growing crystal structures of the semiconductor, since the crystals are three dimensional, they achieve a better volume to interface ratio as compared to the two dimensional multilayered junction Figure 7b [23].

Spheres have the highest volume to interface ratio so using those can increase the interface surface substantial, but it is hard to get them well ordered with enough voids for the opposite semiconductor (Figure 7c) [24, 25]. By use of nanowires it is easier to control the voids of the opposite semiconductor making sure there is an optimum, however most of the nanowires are synthesised on a way that the wires are randomly ordered (Figure 7 d and e) [1, 26-28]. Increasing the volume to interface ratio for the wires can be done by making the wires hollow or combining them with spheres, spheres can be distributed on a better way with the use of nanowires increasing the space for the opposite semiconductor. Do not forget that often one or only a few of these structures are applicable to the desired material.

In this thesis vertically standing p-type nanowires are prepared; the voids between the wires are filled with n-type resulting in a p-n junction as in Figure 7 b. As mentioned previously in this section the solar cell cannot be made as thick as you would like to absorb a high percentage over the entire spectrum. This was because if the solar cell is made too thick, charge carriers generated far away from the depletion zone do not contribute to the photogenerated current. This is overcome by the use of the nanowires, since the depletion zone is parallel to the penetrating light the generated carriers are always near the depletion zone. However structural strength of the nanowires is a limiting factor and production costs can limit the most cost efficient thickness.

2.2 Cuprous Oxide (Cu₂O)

Interest in Cu₂O as a semiconductor started in the 1920's, as a result of the invention of the Cu₂O rectifier by Grondhal [29]. Photosensitive devices made from Cu₂O were primarily characterised in the 30's, but after 1940 the interest shifted to different materials [29]. Cu₂O is usually formed in a cubic stoichiometric structure, as shown in Figure 8 [30].

Although the theoretical maximum of a p-n homojunction solar cell is only around 12%, the material and production costs are extremely low, with an efficiency of 10%, the cost of power is estimated around 0.6\$/W.p. (Watt/peak) [29]. So it could potentially cut the cost per peak watt of crystalline solar cells in half.

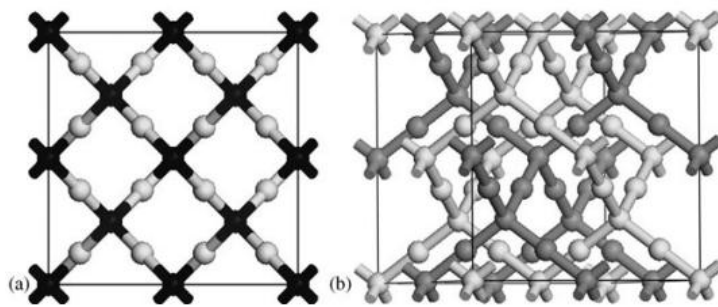


Figure 8 Atomic structure of Cu₂O (a), two interpenetrating Cu-O-Cu networks (b), light spheres are Cu, dark spheres are O.

2.2.1 *p-type*

The most common preparation of Cu₂O is in the form of a p-type semiconductor [23]. Cu₂O gets its p-type character from holes that are formed due to a small amount of Cu⁺ vacancies [30]. This p-type Cu₂O has a band gap of 1.9-2.2eV [17], and has an acceptor energy level 0.4 eV above the valence band [29], which make it interesting for application in photovoltaic cells.

P-type Cu₂O can be prepared by electrodeposition, which is a cheap and simple method offering control over the stoichiometry and thickness of the deposited Cu₂O [19]. For this electrodeposition the most commonly used solution is a 0.02 M Cu₂SO₄ and 0.34 M lactic acid in water. Cu₂O can only be deposited in a limited potential range: between -0.1V and -0.6V for pH 9. For negative potentials out of this range Cu is formed instead of Cu₂O. The morphology of the Cu₂O crystals can be influenced by the pH and the temperature; at a high temperature large micrometer sized crystals are formed while at low temperature small crystallites are formed [19].

The p-type behaviour in Cu₂O originates from Cu⁺ vacancies; these vacancies exist in two different ways: the simple vacancy and the split vacancy. Although the simple vacancy structure is more stable, both structures are possible due to the small energy difference of only 0.06 eV. In the simple vacancy structure, one copper atom is missing, leaving two oxygen atoms behind with only three bonds, see Figure 9a.

But in the split vacancy structure, one copper atom is missing, leaving a vacancy. Now a neighbouring copper atom moves slightly to the vacancy and bonds to the two oxygen atoms left behind with just three bonds. This results in a copper atom bound to four oxygen atoms, which is precisely the structure of copper in fully oxidised Cu₂O. The split vacancy is shown in Figure 9b [7].

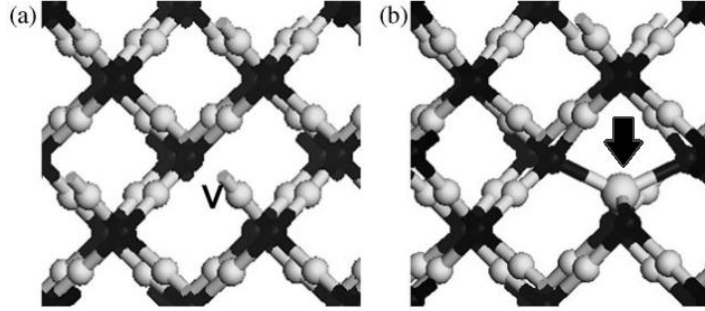


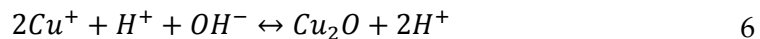
Figure 9: Structure of a single Cu vacancy in Cu₂O. (a) Simple vacancy (b) Split vacancy.

2.2.2 *n*-type

In contrast to p-type Cu₂O which was one of the first known semiconductors, n-type Cu₂O was only first reported in 1986 [31]. This n-type behaviour is still not completely understood. It is proven that it is partly due to the oxygen vacancies as these result in a 0.38 eV donor level below the conduction band, but the 0.16 eV acceptor level is not yet understood [32].

This lack of understanding the n-type behaviour results in the fact that only a few synthesis procedures are known to date. When using electrodeposition, it has been shown that in acidic (pH<7.5) aqueous solutions of 0.4 M copper(II)sulphate and 3 M lactic acid, n-type Cu₂O is formed while p-type Cu₂O is formed at a pH higher than 9 [20]. Solutions of 0.02 M Cu(NO₃)₂ or 0.02 M Cu(CH₃COO)₂ and 0.08 M acetate buffer (pH 4.9) can be used resulting in cubic Cu₂O crystals or dendritic growth respectively [23], with a pH below 6 results in n-type Cu₂O and above in p-type Cu₂O.

The pH dependency found for the different solutions is explained by the governing reaction equation (eq. 6). In an acidic solution, there is a low concentration of OH⁻, so the stoichiometric ratio of copper and oxygen atoms can be larger than 2:1, which results in n-type Cu₂O. So the oxygen vacancies are due to the lack of OH⁻ [33]. As is the opposite at alkaline solutions, the high concentration of OH⁻ results in Cu⁺ vacancies giving it its p-type properties.



A different way of producing n-type Cu₂O is by just boiling a thoroughly cleaned copper sheet in a 10⁻³ M CuSO₄ solution [21], but its pH dependency has not been researched extensively for this method, only a pH drop from 5 to 3.5 has been observed.

2.3 Nanostructure synthesis

Nanostructures are defined as structures that are in at least two dimensions maximum 100nm in size. Several kinds of nanostructures are possible i.e. nanorods, nanotubes, nanospheres, nanowires and nanocubes. These nanostructures, especially the one dimensional structures (tubes, rods and wires) are interesting to investigate for the use in solar cells due to their high volume to surface ratio, as is described in section 2.1.4.

Several techniques can be used for synthesising these nanostructures, which can be divided into two categories: vapour phase and liquid- or solution based techniques [34]. In the solution based techniques a division can be made between template and template free methods. For synthesizing Cu_2O nanowires, commonly template solution-based techniques are used [1, 27, 28]. In the template-based method, templates provide 1-D channels for guiding the growth of materials in the 1-D form. The deposition in or at these channels can be done by various methods i.e. electrodeposition, sol-gel, chemical vapour deposition and electroless deposition [34]. When the template free method is used, often more stringent growth conditions are required, to ensure 1-D growth over the entire material.

2.3.1 Template types

The template based methods can be divided into three categories depending on the type of template used: negative template, positive template and surface step template. The negative template is used most commonly, as is also in this research.

In the positive template method, 1-D nanostructures are used as templates on which the material is deposited for nanowire synthesis. These 1-D nanostructures can be made from carbon nanotubes, DNA or polymer. This technique is schematically shown in Figure 10a. [24]

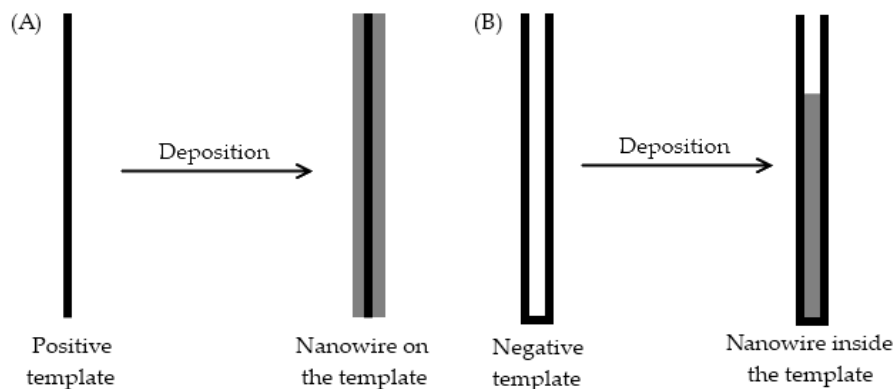


Figure 10: Schematic view off (a) Positive and (b) Negative template deposition.

With the negative approach, a prefabricated hollow structure is used to deposit the material inside the hollow pores. This is schematically shown in Figure 10b. The two most used templates are track etched membranes (TE) and alumina membranes (AAO). Templates can also be made from diblock copolymer, nanopores in glass and other porous or hollow structures. In this research track etched

membranes from polycarbonate are used (PCTE). These membranes are made by shooting heavy charged atoms, i.e. Ni or U at 30 MeV through polycarbonate, which leaves a damaged hollow path. This path has a diameter of minimal 2.5 nm and by chemical etching the pores are broadened to the required thickness.

The third and less commonly used type of template is the open planar surface, composed of stacked planes which are highly oriented. The atomic scale steps of this template are used as the template to grow nanowires. Materials as, graphite and mica can be used for this kind of template.

2.3.2 Templated electrodeposition of Cu_2O

The two most commonly used template assisted deposition methods are: electrodeposition and sol-gel synthesis. Each of these methods works better with a specific type of template for a certain type of material.

In electrochemical deposition, the working electrode (where the deposition is done) is the prefabricated template or a conductive support for the template. Electrodeposition is often carried out in a standard three electrode setup containing: the working electrode, counter electrode and a reference electrode. The advantage of three electrode setup is that the potential is set with reference to the reference electrode, the reference electrode has a fixed and stable potential to the working electrode, giving reproducible results. A potential more negative than the standard redox potential is applied to the working electrode delivered by an external potential supply, the potentiostat, while more the positive terminal is connected to the counter electrode. The three electrodes are immersed in a solution (the electrolyte) containing the metal ions to be deposited, as shown in Figure 11. This setup is also used in this research for electrodepositions that are performed. [34, 35]

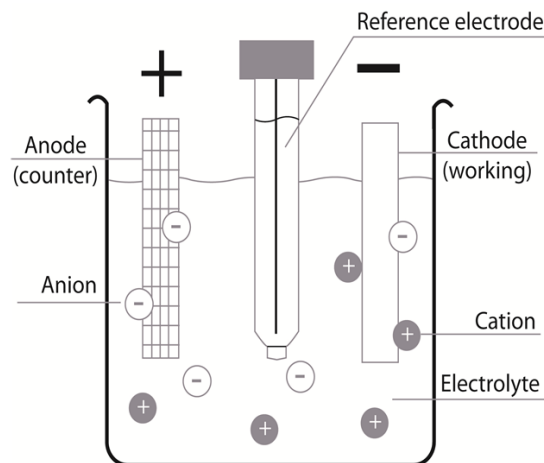


Figure 11: The standard three electrode setup.

Most commonly negative templates of PCTE or AAO are used for templated electrodeposition. These templates require a support of a conducting layer at the back of the membrane to serve as a working electrode. In this research a gold layer is used as back electrode on polycarbonate membrane.

One of the advantages of electrodeposition is the ability to have a good control over the nanowire length, by selecting the deposition time. Another

advantage is that it is a low temperature, inexpensive process, and it allows fabricating vertical, free standing, and dense nanowire arrays. A disadvantage of electrodeposition is that a conductive substrate is necessary, which limits the range of materials that can be used. Another disadvantage is that it is hard to deposit in pores with a very small diameter of a few nanometres in diameter. However this problem can be overcome by using pulsed deposition, after each potential pulse, a delay follows, leaving time for the ions to diffuse into the region where deposition occurs. [34, 35]

For the deposition of p-type Cu_2O a solution of CuSO_4 is used at a constant potential. However in some applications a pulsed deposition can be useful to get deposition in locations, not possible with a constant potential due to diffusion limitations. For the deposition of n-type Cu_2O copper(II)acetate is used as source for the Cu^{2+} ions. Deposition of Cu_2O requires two steps, the reduction of Cu^{2+} ions to Cu^+ ions (eq. 7) and deposition of Cu^+ as Cu_2O (eq. 8). Due to H^+ formed during deposition, the electrolyte will gradually get more acidic.



Important to note is that (eq. 8) is an equilibrium reaction, thus in an acidic environment the deposited Cu_2O is dissolved. The deposition of n-type Cu_2O takes place in an acidic environment so its deposition speed is much slower than that of the p-type. In both cases care should be taken in removing the sample as fast as possible limiting the amount of dissolution.

2.3.3 Template free electrodeposition of Cu_2O

Absorbent assisted deposition method is based on templated electrodeposition, but no template is used. Instead, absorbents are added to the electrolyte. These absorbents absorb preferentially to specific crystal planes, dramatically slowing down the crystal growth in this direction. This technique has been proven to be applicable for n-type Cu_2O deposition, i.e. by the addition of Cl^- ions the $\{100\}$ planes are blocked, while adding sodium dodecyl sulphate (SDS) absorbs on the $\{111\}$ plane which are blocked in this case [36]. Some of the possible crystal structures of Cu_2O possible with absorbent assisted electrodeposition are shown in Figure 12.

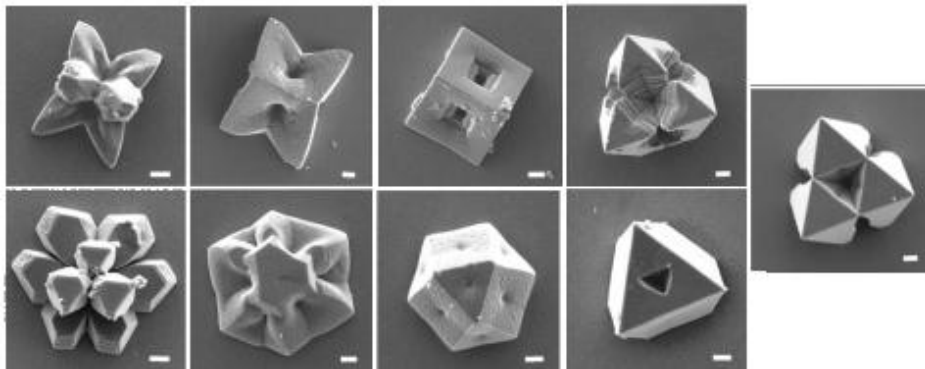


Figure 12: Several crystal structures possible with absorbent assisted electrodeposition.

McShane et. al. have shown that with the use of a buffered solution the pH can be kept constant near the working electrode, regardless of the deposition rate [23]. This is important since H^+ is formed at the deposition and thus decreases the pH, this decreased pH results in the absorption of any dendritic branches of Cu_2O . Using constant pH makes it possible to facilitate dendritic branching, which increases the interface significantly compared to a normal thin layer of Cu_2O . This dendritic branching of Cu_2O is shown in Figure 13.

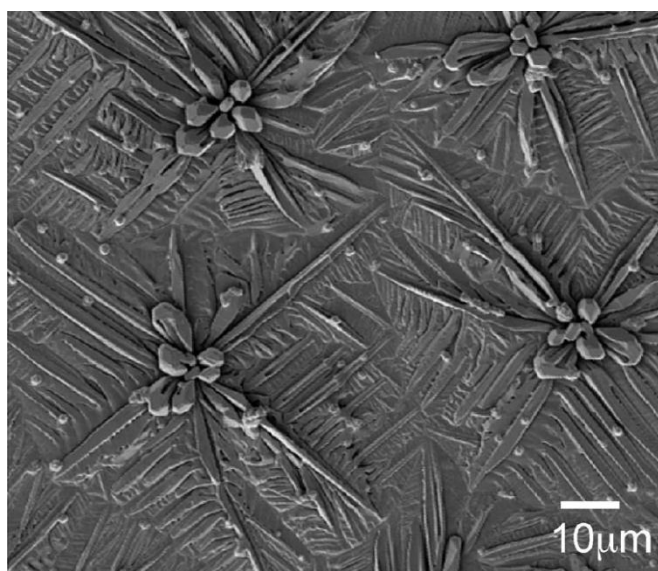


Figure 13: Dendritic growth of Cu_2O .

3 Experimental details

3.1 Chemicals used

All chemicals used were purchased from commercial sources and without any further purification. Sodium hydroxide (KOH, 90%), acetic acid (CH₃COOH, 99.7%), copper(II)acetate (Cu(CH₃CO₂)₂, 99%) and sulfuric acid (H₂SO₄, 96%) were purchased from Acros Organics. Potassium hydroxide (NaOH, >98.5%) and copper(II)sulphate pentahydrate (CuSO₄ · 5 H₂O, 9.995%) were purchased from Sigma Aldrich. Lactic acid (C₃H₆O₃, >88%) was purchased from Fisher Scientific. Dichloromethane (CH₂Cl₂, 99.8%) was purchased from Boom Chemicals. Ethanol (CH₃CH₂OH, 99.8%) was purchased from Assink Chemie. Distilled water was used in all the experiments.

3.2 p-n homojunction solar cell preparation

The preparation of the p-n homojunction Cu₂O solar cell is done in six consecutive steps. The preparation starts with a polycarbonate membrane, on which a back electrode is sputtered with gold. Next is the electrodeposition of the p-type Cu₂O nanowires in the pores. Free standing nanowires are left after dissolution of the membrane. An extra p-type deposition is done to form a bottom layer of Cu₂O, which ensures no short circuit is formed between the p-type and the n-type Cu₂O by the gold back electrode. By depositing n-type Cu₂O on top of the bottom layer the p-n junction is formed. The last step is to deposit an ITO top contact on the solar cell by pulsed laser deposition. The different steps will be explained in the following sections and are shown in Figure 14.

3.2.1 Sample preparation (A+B)

Nuclepore™ track-etched polycarbonate membranes purchased from Whatman were used in all experiments. The pores of the membrane have a diameter of 200 nm at the base but have a cigar like shape resulting in a broader middle; the membranes have a thickness of 10 μm and a total diameter of 25 mm. A gold layer of ~200 nm is coated on one side of the membrane using a Perkin-Elmer 2400 sputtering system on the following settings: a background pressure of 0.8·10⁻⁶ torr, a deposition pressure of 2·10⁻² mBar, a power of 75W and a potential of -750 V. Resulting in a growth rate of a proximally 12.5 nm per minute; in 16 minutes the 200nm layer was sputtered. The sputtering is performed at this relatively low growth speed to ensure the membrane is not heated too much, so only few deformations of the membrane occur. This gold layer on the back of the membrane is used as the working electrode.

With a piece of glass a water tight seal is made between the electrolyte and the gold back electrode. This is important to prevent the deposition from taking

place at the back of the working electrode (sputtered gold) instead of in the pores. The sample is finished by making a contact between the gold and the working electrode of the potentiostat using copper adhesive tape.

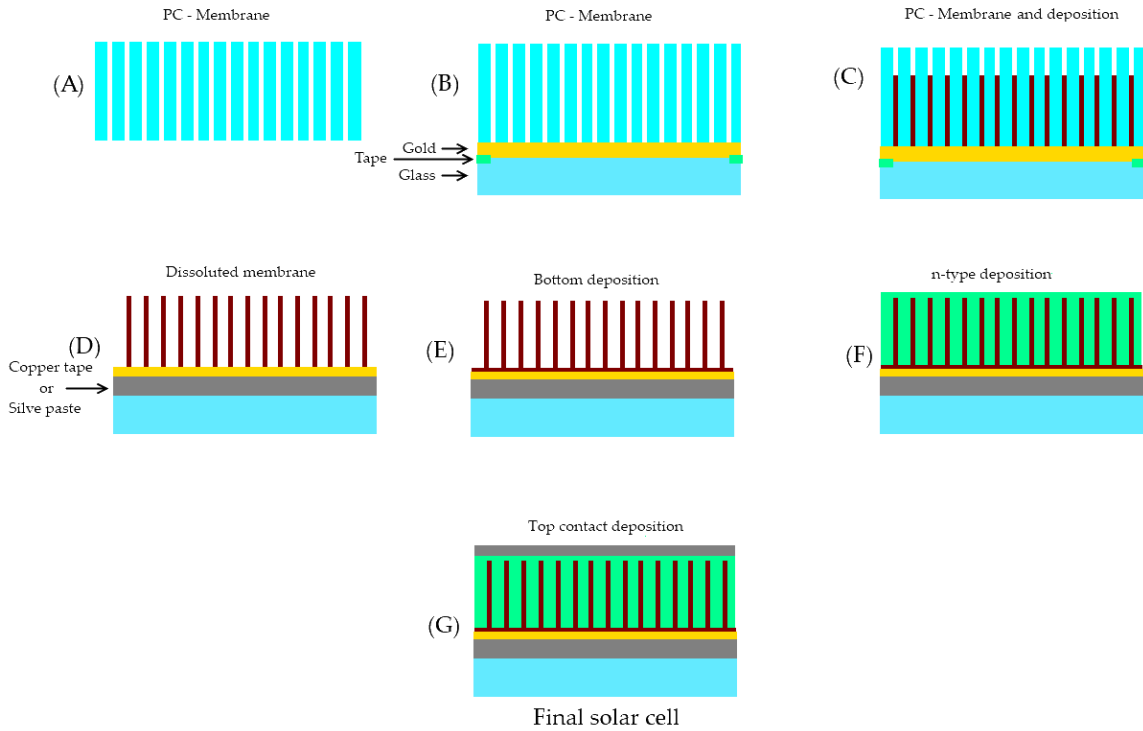


Figure 14: Schematic representation of the steps taken in the solar cell synthesis.

3.2.2 Nanowire deposition (C)

The wires of p-type Cu_2O are grown in the pores of the membrane using templated electrodeposition. A standard three electrode setup is used in combination with an Autolab 128N potentiostat, where the sputtered gold on the back of the membrane acts as the working electrode. The wires are grown from an aqueous solution of 0.02 M CuSO_4 and 0.4 M lactic acid, with the pH adjusted to 11 by using NaOH (or KOH) and H_2SO_4 [3]. Since the solution is not buffered, the pH should be checked before each deposition. The wires are grown at 60 °C and at 0.4V with respect to a Ag/AgCl reference electrode. The length of the nanowires can be varied by changing the deposition time.

3.2.3 Template dissolution (D)

After deposition of the nanowires in the pores of the membrane, the membrane has to be dissolved, leaving free standing nanowires. Since the sample will loose its strength when the membrane is dissolved, it is stuck to a new glass slide, this time binding the entire surface with silver paste or copper tape. During the dissolving process there are only three criteria: the wires are not allowed to break, the sample has to stay intact and all of the polycarbonate has to be dissolved. If all of these criteria are met, deposition of the bottom layer is possible at the gold.

The membranes were dissolved in Dichloromethane (CH_2Cl_2). During the experimental work the dissolution step was found to be the most difficult step. This has resulted in the investigation of many different methods for dissolving the membrane with CH_2Cl_2 . Variations have been made in dissolution time, dissolution temperature, flow in the dichloromethane, position of the sample (i.e. angle, flat or upside down) and nr of times washed.

3.2.4 *Bottom deposition (E)*

After dissolution of the membrane, the bottom deposition can be executed, for this step no adjustments have to be made to the, only extra Teflon tape is added on the copper tape or silver paste, to ensure no deposition takes place on these materials.

For the deposition the same solution was used for this deposition as for the wires, since p-type Cu_2O is required again. However the requirements are more stringent now, a complete bottom deposition is required to achieve a p-n junction with no short circuit. The bottom layer is undesirably deposited on the tops of the nanowires making it challenging to deposit a complete bottom layer; also thin layers of insoluble polycarbonate are left which make it even harder for bottom deposition. By means of pulsing extra bottom deposition is attempted to be achieved.

3.2.5 *Void deposition (F)*

For the electrodeposition of n-type Cu_2O between the wires and on top of the bottom layer, a solution of 0.02 M Copper(II)acetate and 0.08 M acetic acid is used with the pH adjusted to 4.9 with NaOH (or KOH). The electrodeposition was carried out at a temperature of 70 °C and at a potential of +0.02V with respect to a Ag/AgCl reference electrode.

3.2.6 *Top contact deposition (G)*

For the top contact a 100 nm layer of ITO is deposited by pulsed laser deposition on top of the solar cells. For this deposition a spot size of 3mm² was used, the sample was placed 5 cm from the target, an energy density of 2.5 J/cm, a deposition pressure of 0.015 mBar of O_2 and 10 Hz were used as settings to deposit a 200nm layer in 3 minutes.

3.3 **Sample inspection**

After each of the previous mentioned steps the samples were inspected first in a low resolution JEOL 6490 SEM, equipped with a tungsten electron gun. When further inspection was required the samples were inspected with a high resolution LEO1550, equipped with a field emission gun. It was important to inspect the sample after each step so it is clear which steps are the bottleneck and need to be improved. An important difference is that the JEOL SEM is less capable in detecting organic material compared to the LEO SEM.

3.4 Sample characterisation

Characterisation of the solar cells was carried out at the Materials for Energy Conversion group of the TU Delft. The characterisation is done at two points in the production process, the photocurrent of just the wires is measured and of the final solar cells. For both of the measurements an Oriel Sol3A 94023A (class AAA) was used, emitting the AM 1.5 solar spectrum, at 1.0x the power of the sun delivering 100mW/cm².

3.4.1 Nanowires photocurrent measurement

Photocurrent characterization was carried out in a three electrode cell, in which the counter electrode was a platinum wire, the working electrode the synthesised nanowires and the reference electrode a Ag/AgCl electrode. The solar cell was placed in a custom made cell, in which the sample was secured behind a 6 mm round opening. A contact was made on the solar cell by a thin silver wire which was attached to the silver paste between the gold layer and the glass. A compartment in front of opening was filled with the electrolyte, for this electrolyte an aqueous solution of 0.02 M Na₂SO₄ was used, the pH was not adjusted and had a value of 5.4. A schematic overview of the used setup is shown in Figure 15.

Chrono amperometric measurements were carried out at a constant potential of -0.2 V with respect to a Ag/AgCl electrode. The measurements were taken for a time of 20 minutes, starting in the dark for 200 seconds; after which the cell was illuminated for 100s and 100s in the dark consecutively for the remaining time. The photocurrent is determined by the difference between the generated current when the light is off and on.

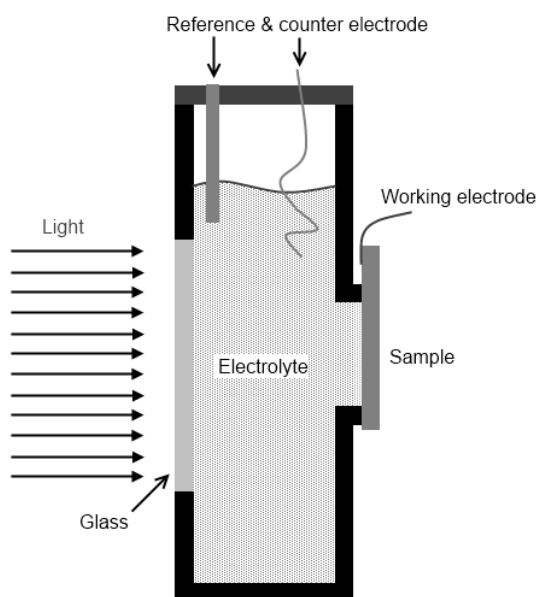


Figure 15: Schematic representation of the setup for the photocurrent measurement of the nanowires

3.4.2 *Solar cell photocurrent measurements*

Photocurrent measurements of the solar cells were carried out by a linear voltage sweep; the potential sweep went from -0.5 V to +0.5 V, in 1000 steps of 1mV in 200 seconds. First a complete sweep was performed in the dark, followed by a complete sweep with the cell being illuminated. In an ideal case this would lead to a measurement result as shown in Figure 4.

For these measurements the setup used for the nanowire photocurrent measurements cannot be used. A simple measurement platform has been developed, which consists of a plastic plate with two copper contact pads attached, this was done by screws so it is possible to move them freely around to connect the sample, as is shown in Figure 16. One of the contact pads is put on top of the ITO top layer, while the other one is connected to bottom electrode.



Figure 16: The developed measurement platform.

4 Results and discussion

In this chapter, the results of the experiments are presented, including the discussion of these results. Firstly the different preparation routes will be evaluated including Scanning Electron Microscope (SEM) images of the results after the different preparation steps. Secondly the measurement results of the photocurrent for the nanowires and the solar cells will be discussed.

4.1 Preparation process of the p-n homojunction

In this part of the results and discussion, the results of the different tested preparation processes are presented and discussed. First the results of the sample preparation are shown and next the electrodeposition of the nanowires, the dissolution of the membrane, the bottom deposition, the n-type deposition and the deposition of the top electrode will be treated.

4.1.1 Sample preparation

The preparation process starts by sputtering a gold layer on the polycarbonate membrane. A first batch of membranes was prepared with a 50 nm layer, during dissolution of the membrane, this gold layer found to be too weak and ruptured at almost all of the samples.

A second batch of membranes was prepared with a 200 nm layer of gold, which was done on a much lower growth speed ensuring no deformation of the membrane would occur due to heating. The sputtering was executed on a power of 75 Watt and a potential of 600-800 Volt, resulting in a growth speed of ~12.5 nm. Figure 17 shows the resulting gold layer. This thicker layer has proven to be of sufficient thickness to withstand the dissolution process.



Figure 17: Result of the 200nm sputtered gold layer (after deposition and dissolution of the membrane)(HR)¹.

¹In case of a SEM image the addition of (HR) and (LR) tells which SEM has been used, the LEO 1550 or the JEOL6490 respectively (section 3.3).

A second challenge during the sample preparation was the release of the glass slide during deposition. This came from the alkaline character of the electrolyte, which was responsible for the dissolution of the adhesive of the tape. This was easily solved by folding an extra layer of Teflon tape around the sample. Although the glue of this tape was also slowly dissolved but it gave enough time to complete the deposition.

With the Teflon tape folded around the sample, some minor electrolyte leakage was present through the corners of the sample. This leakage gave no problems since the Cu^+ ions are quickly deposited on the back electrode after which only new ions are supplied by diffusion through the small pores at the corners.

In Figure 18, the best method to prepare the sample for electrodeposition is shown. The figure shows the extra layer of Teflon tape used, the gold layer isolated from the electrolyte by the glass and the copper tape used as contact between the gold back electrode and the electrode of the potentiostat.

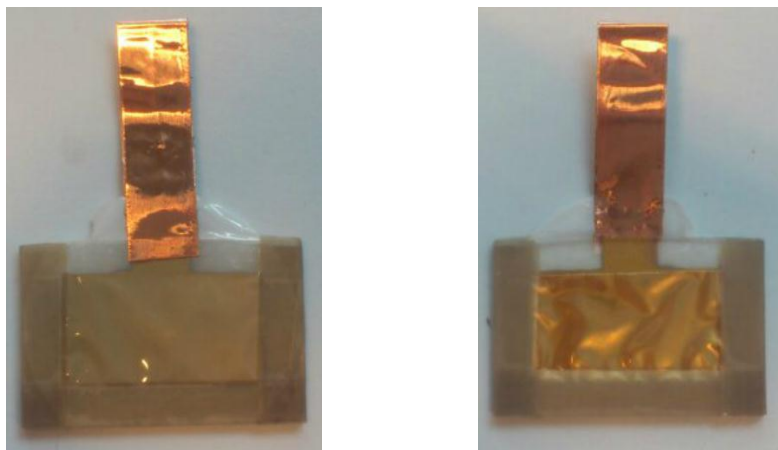


Figure 18: Photograph of the sample before deposition, front side (left) and back side (right). On the front side the membrane pores are opened, while on the back side you can see the gold covered by the glass slide.

4.1.2 Nanowire electrodeposition

Nanowire deposition was successful and billions of free standing nanowires could be created, as shown in Figure 19. For a deposition time of 7 minutes nanowires with a length of 1.3-1.5 μm were grown as is shown in Figure 20. But often many nanowires were washed away during the dissolution of the membrane, by decreasing the length to diameter ratio to 5:1 the structural strength is increased. Since the nanowires have a diameter of 200 nm, the wires are grown to a length of 0.8-1 μm by decreasing the deposition time to 4 minutes. The results of the decreased deposition time are showed in Figure 21 a-c.

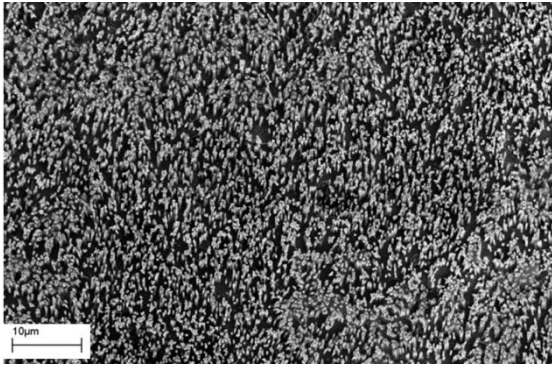


Figure 19: Thousands of free standing Cu_2O nanowires (HR)¹.

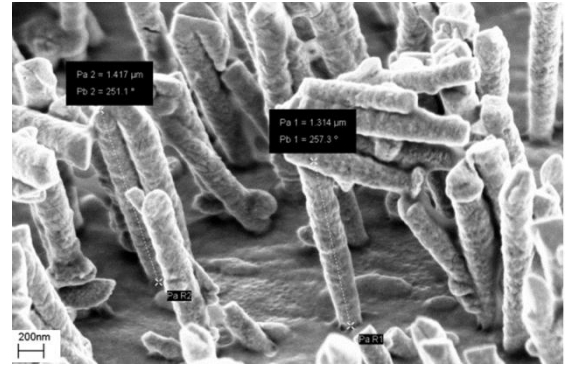


Figure 20: 1.3-1.5 μm nanowires resulting from 7 minutes of deposition (HR).

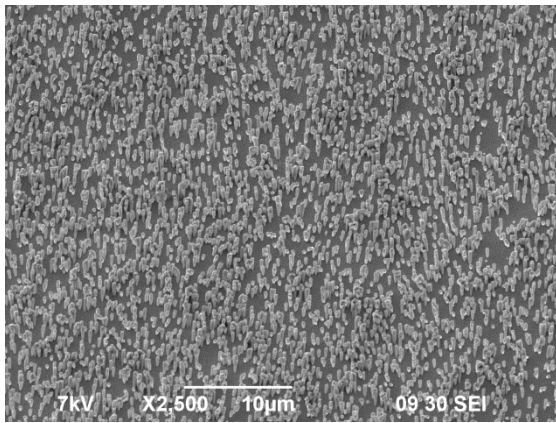


Figure 21a: Overview of a sample deposited in 4 minutes (LR).

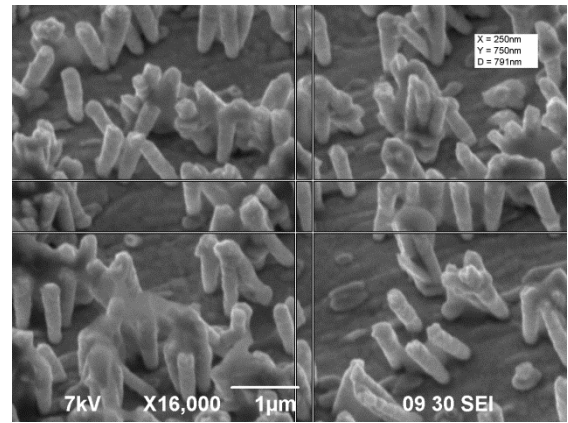


Figure 21b: A nanowire of 0.8 μm grown in 4 minutes (LR).

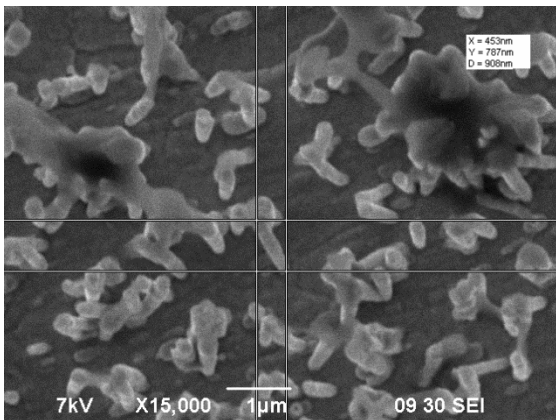


Figure 21c: A nanowire grown in 4 minutes (LR).

4.1.3 *Template dissolution*

Unexpected at the start of this research, but the dissolution of the template was found to be the bottleneck of the preparation of p-n homojunction Cu₂O nanowire solar cells. The challenges at this step came from three directions: the strong organic dissolution capabilities of dichloromethane (CH₂Cl₂), the structural weaknesses of the nanowires and thirdly difficulties in dissolving the entire template. These three challenges will be discussed and the found solutions are presented.

The strong organic dissolution capabilities of the Dichloromethane are necessary for dissolving the membrane. The difficulties of this characteristic came from the copper tape, specifically the glue of the copper tape. The glue of the copper tape is an organic compound and thus dissolved by dichloromethane, resulting in slow release of the sample in the dissolution step. Consequentially the dissolution times were limited (max. 20 min.) as well as the possibilities regarding flow in the solvent and orientation of the sample during dissolution.

This was resolved by using silver paste instead of the double sided copper tape. Although the silver paste was initially used to solve the problem of glue (from the copper tape) leaking through the gold layer by capillary forces, it also solved the problem of sample release. The silver paste was not dissolved by the dichloromethane, leading to the capability of much longer dissolution times; up to several hours. As well as the possibility of different orientations i.e. angle and upside down and flow in the solvent without release of the sample.

With the increased stability of the sample, longer and harsher dissolution and washing methods were tested. Unfortunately, the nanowires were found extremely fragile inclining that no flow in solvent was possible without breaking all or a large part of the nanowires.

The structural strength of the wire was tried to be increased by shortening the wires, so less forces would work on them when flow would be present in the solvent. This solution has also been treated in the previous paragraph about the electrodeposition; decreasing the length to <1 μm. Unfortunately, this decreased length had no significant effect on the structural strength and thus the chance a sample would still contain nanowires after the dissolution step.

The goal of the dissolution step is to dissolve the entire template, leaving no traces of polycarbonate on the sample. Having dissolved the complete template a clear gold surface should be left on which the bottom deposition can take place. Unfortunately this goal was not achieved in the dissolution step, although many different methods have been tried. These methods will be discussed next and results will be shown with Scanning Electron Microscopy images.

The first method tried was a dissolution time of 20 minutes at room temperature. Free standing wires are visible in Figure 22, but also rather much polycarbonate is left between the wires (as clarified with the red circles). By the dark colour of the bottom it can be recognised that there is also a layer of polycarbonate (PC) at the bottom.

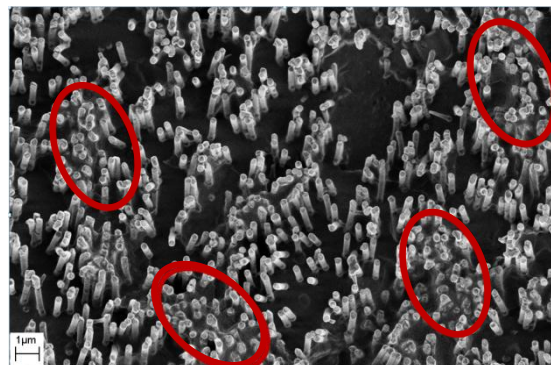


Figure 22: SEM image of a sample, dissolved with CH_2Cl_2 at a temperature of 21 °C for 20 minutes (HR).

By increasing the dissolution time to 40 minutes more polycarbonate is expected to be dissolved, however results show no or little difference (Figure 23). Due to the use of copper tape at this point, most of the samples did not stay intact using this longer dissolution time and were folded or floating.

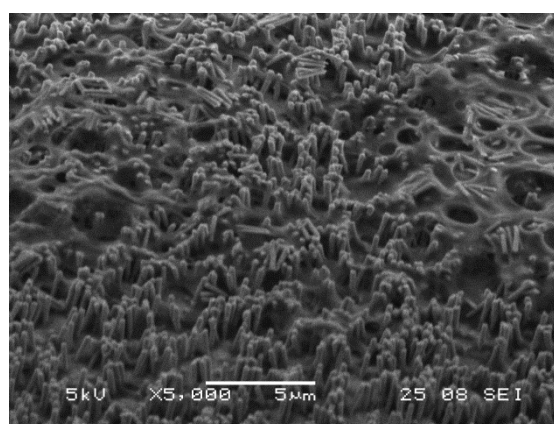


Figure 23: Sample dissolved with CH_2Cl_2 at a temperature of 21 °C for 40 minutes (LR).

By introducing flow in the Dichloromethane, it was tried to dissolve more CH_2Cl_2 . This was done by spurting with a Pasteur pipette, slowly stirring the sample in the solvent and by adding a magnet stirrer on low RPM. Unfortunately with this dissolution method, almost all of the samples broke and for the few that stayed intact all the wires were flushed away.

The only positive remark is that the polycarbonate has been removed to a higher degree. The result is shown in Figure 24.

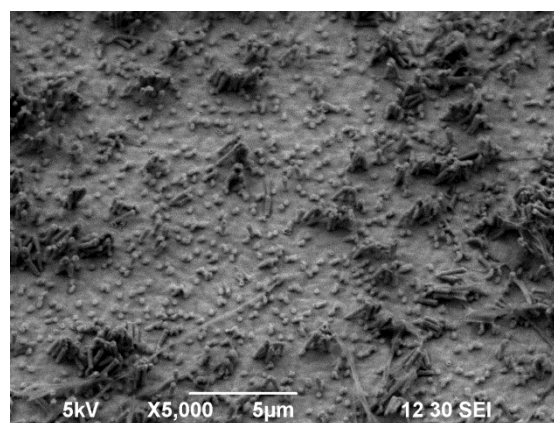


Figure 24: Sample dissolved under induced flow for 20 minutes at 21 °C (LR).

The temperature of the Dichloromethane is increased from room temperature to 40 °C. This has several advantages; due to a temperature gradient over the solvent a little flow will be present, the solubility equilibrium will be higher and diffusion will be faster.

The increased temperature had a positive effect on the amount of template dissolved, it is dissolved to a significantly higher degree than at room temperature and most of the wires are still intact. The result is shown in Figure 25; the improvements are clearly visible if compared to Figure 22.

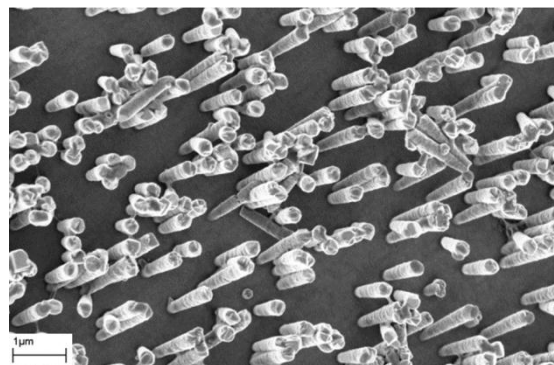


Figure 25: Sample dissolved with CH_2Cl_2 at a temperature of 40 °C for 20 minutes.

After the dissolution process at 40 °C, the template looks dissolved to such a degree that bottom deposition would be possible. However during the second deposition the Cu_2O is deposited on top of the wires, as will be discussed in section 4.1.2. This deposition on top of the wires is a sign that the polycarbonate template is not completely dissolved and thus acts as an insulating barrier between the gold and the electrolyte.

Further inspection is carried out to find any evidence of such a polycarbonate layer on top of the gold layer. This layer is indeed found as is shown in Figure 26, a polycarbonate layer with a thickness of ~40nm was found.

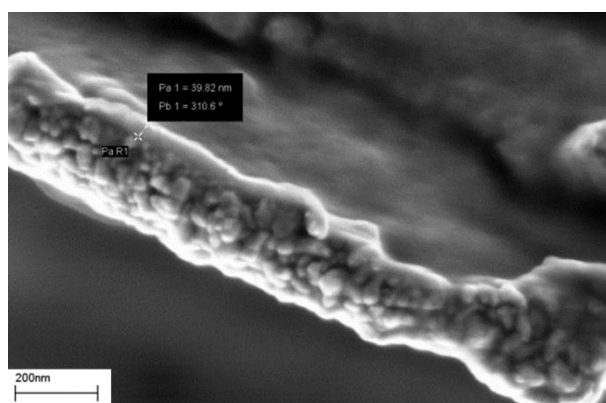


Figure 26: The polycarbonate layer left behind after the dissolution process (HR).

With the use of silver paste dissolution times could be enhanced to up to one hour. However dissolution for 1 hour at the high temperature had no noticeable effect on the amount deposited on the tops, neither did washing under an angle and multiple times.

4.1.4 Bottom layer deposition

In the previous paragraph, the unfortunate deposition on the tops instead of on the bottom was shortly mentioned. While assumptions were made that the template was dissolved to such a degree that bottom deposition was possible, it was found that this was not the case. In the deposition that was carried out in 3 minutes, cubic shaped Cu_2O crystals were formed on top of the wires. After deposition, also a strange organic layer was found on top of the wires. The wires with second deposition on top of the nanowires with the strange organic layer is shown in Figure 27, in the left picture the cubic shaped crystals on top of the wires are clearly visible while in the other picture the organic layer is visible, copper tape was used to adhere the sample.

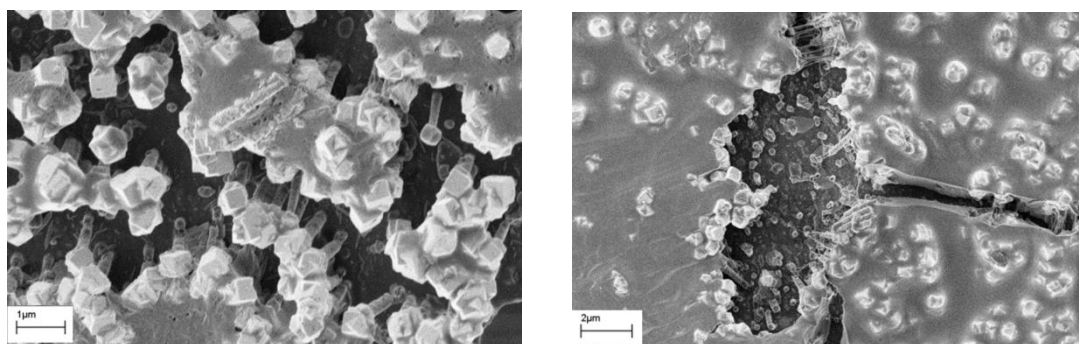


Figure 27: The sample after the "bottom" deposition, on top of the wires (HR).

Energy-dispersive X-ray spectroscopy (EDX) showed that the layer on top of the nanowires is an organic layer. It was assumed that the layer was the bottom layer of the residual PC membrane, which came to float and was then stuck between the cubes of the wires. However attempts to dissolve this top layer with Dichloromethane, acetone, ethanol and water did not have any effect.

Since the layer is not dissolved in Dichloromethane and a difference in the EDX between the top layer and bulk PC membrane, it probably is not the residual polycarbonate. In the preparation of the sample, no organic compounds are used, however the glue of the different used tapes is organic. Tape was used for bonding the sample to the glass sheet, to prevent deposition on the substrate during second deposition and copper tape was used as contact between the gold and the electrode.

The layer is found over the entire sample, leading to the theory that glue of the copper tape is leaked through the gold layer due to capillary forces. This is possible because the gold is sputtered on the membrane but the pores of the membrane are not completely covered, so if a wire is broken or not grown at all it is possible for the glue to leak through it.

This theory was tested by changing the copper tape with, silver paste, since this silver paste consists of silver flakes it is not possible for it to leak through the pores. The first samples look promising, with much less organic layer on the wires and also some deposition on the bottom occurred. Figure 28 shows two SEM images on the left one the bottom deposition is shown, although it is only local there is a

spot that has a fully covered bottom by multiple crystals. On the right image, no organic layer can be found. Another advantage of the silver paste was that it is not dissolved in the CH_2Cl_2 as mentioned in section 4.1.3.

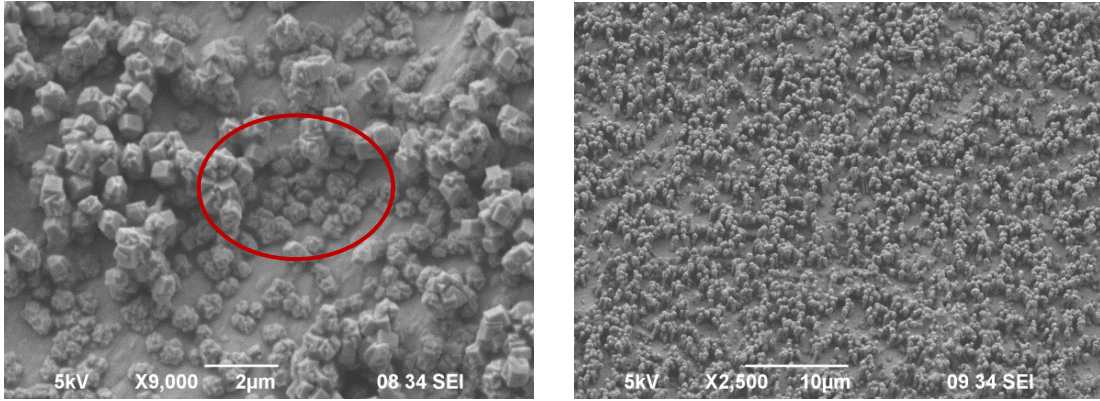


Figure 28: Bottom deposition found on the silver paste sample (left) and the absence of the organic layer (right) (LR).

However, for other samples prepared the organic layer was found again on the tops, although in a lesser degree than for the samples with copper tape. The organic layer thus did not come solely from the copper tape, two options are left for the source of the organic layer: the Teflon tape and the copper tape used as connector. Due to time limitations of this research no preparation route without the use of any of these possible sources was investigated.

It was tried to enhance electrodeposition on the bottom by use of pulsed deposition, leaving time for the copper ions to diffuse to the bottom. However, this did not result in bottom deposition, the wires were covered with smaller crystals and for more length instead of only at the top (Figure 29).

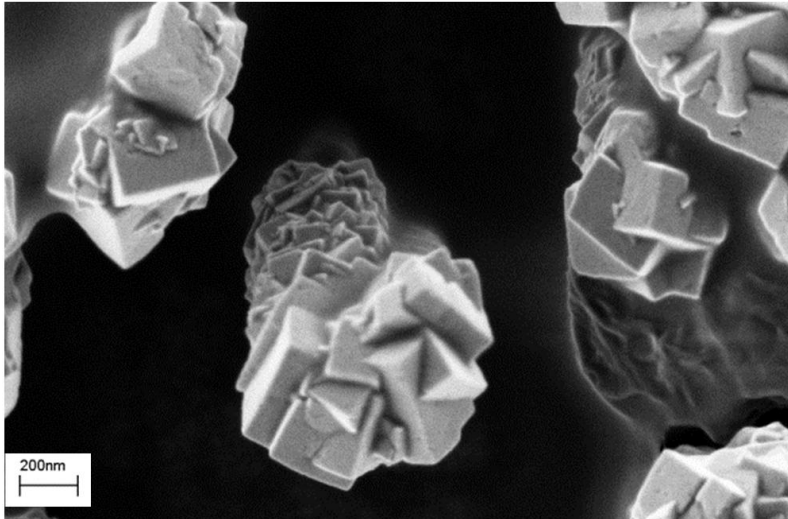


Figure 29: Nanowire partially covered with p-type Cu_2O by pulsed electrodeposition (HR).

4.1.5 *n*-type deposition

The deposition on the bottom was probably not feasible due to a residual layer of the polycarbonate membrane. As this polycarbonate layer is non conductive, it should be possible to use the residual layer as an insulator preventing short circuit between the bottom contact and the *n*-type Cu_2O , instead of a *p*-type bottom layer. This idea lead to investigation of a preparation route with no bottom layer of *p*-type Cu_2O but instead using the residual polycarbonate as an insulating layer and directly depositing the *n*-type Cu_2O on top and between the wires.

For the *p*-type deposition, more coverage of the wires was found, by using pulsed electrodeposition so also pulsed electrodeposition was used for depositing the *n*-type Cu_2O . By depositing the *n*-type in pulses high coverage of the wires was tried to be achieved, after these pulses, a potential was applied for a longer time growing a closed top layer.

For the first sample with *n*-type deposition several short pulses were followed by one longer applied constant voltage. A layer was formed that was far from complete on the wires as shown in Figure 30. Also rather much deposition occurred on the bottom.

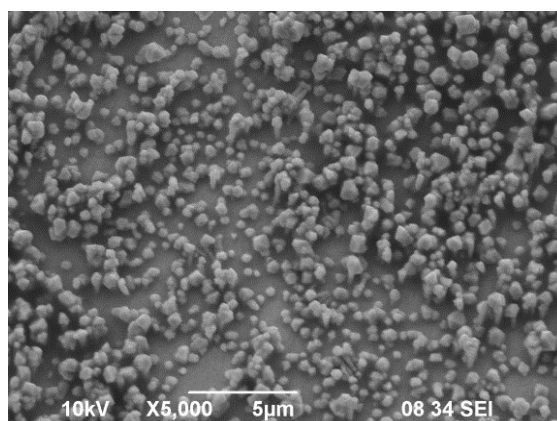


Figure 30: *n*-type Cu_2O deposited by 10 pulses of 10s with 10s of rest and one constant pulse of 120s (LR).

By increasing the deposition time of the constant potential pulse significantly, the *n*-type top layer was uniform to a higher degree, as is shown in Figure 31. The number of short pulses before the long pulse was decreased for less bottom deposition.

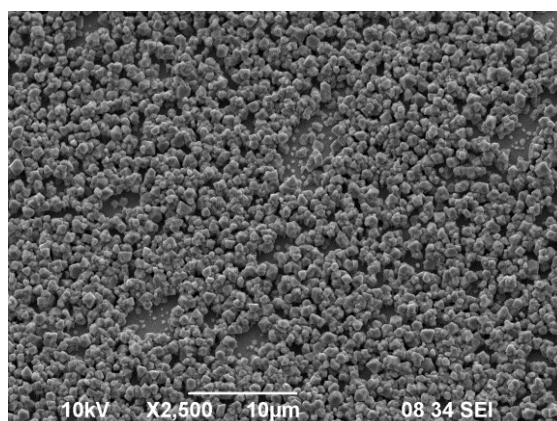


Figure 31: *n*-type Cu_2O deposited by 5 pulses of 10s on and off, followed by one constant pulse of 1500s (LR).

By adding some short pulses after the constant potential pulse, it was tried to fill the holes that are still present on Figure 31. Due to the rest time between the pulses, ions can diffuse in these holes and thus deposit in them. This indeed led to a more uniform layer of n-type Cu_2O on top of the wires.

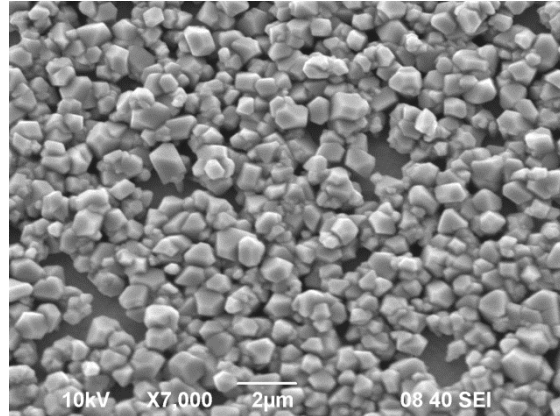


Figure 32: n-type Cu_2O deposited with 5 pulses of 10s off and on followed by one constant pulse of 1500s and then again 5 pulses of 10s on and off (LR).

Finally the long pulse was split into two pulses leading to an extra nucleation step in the deposition. This is done to achieve more equal sizes of crystals. Also the deposition length of the pulses at the end was slightly increased. The result is a more continuous layer of n-type Cu_2O on the nanowires, with large areas fully covered, as shown in Figure 33.

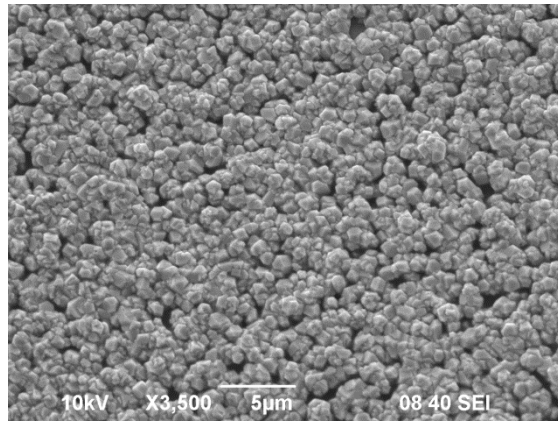


Figure 33: n-type deposited with 5 pulses of 10s on and off followed by two pulses of 800s with 10s off and then finished with 5 pulses of 15s on and 10s off (LR).

It was possible to grow a rather homogenous layer of n-type Cu_2O on top of the nanowires. However, the samples always have some spots with no or very few nanowires, where it was not possible to create a homogenous layer. Due to the long deposition time, some crystals grow until the bottom, which can cause a short circuit if the polycarbonate layer is not thick enough.

The top contact is deposited on top of this n-type layer, by pulsed laser deposition. Due to the local areas with no nanowires this top layer can cause a short-circuit if the polycarbonate layer is not sufficiently thick enough. To reduce this chance, the sample is divided in four regions by Teflon tape. During the deposition process no ITO will cover the sample where the Teflon tape is, thus four separate regions can be characterised as a solar cell.

4.2 Sample characterisation

In this chapter, the photocurrent measurements will be shown and discussed. Firstly, the nanowire photocurrent in NaSO_4 measurements carried out with chrono amperometry is covered. Secondly, the photocurrent of p-n junctions synthesised with the n-type top layer, measured with a linear sweep voltage, is discussed.

4.2.1 Nanowire photocurrent

Measurements of the photocurrent were successfully carried out at the TU Delft, three different samples with each of them a different amount of nanowires were tested. The three samples had ~80%, ~60% and ~50% of the wires still standing after the dissolution of the template, these amounts were estimated after inspection. The samples used were connected to the substrate with silver paste as described in 4.1, and had a length of $\sim 1\mu\text{m}$.

Measurements showed clear semiconductor behaviour for all of the samples: an increased negative current was observed when the cell was illuminated, which indicates p-type behaviour. The first measurement, of the 50% sample, is shown in Figure 34. The measurement is started in the dark for 200s, then the light is switched on (open arrow) and the current shows a sharp increase, after 50s the current reaches a steady state, at a level more negative (increase in current) than before switching on. After 100s of illumination, the light is switched off (crossed arrow) and a sharp decrease in current was observed, again after $\sim 50\text{s}$ the current is levelled out, now at a less negative value than before switching off. This pattern is found over the entire measurement. The current balances out at a less negative level for each cycle, which is due to the degradation of the Cu_2O .

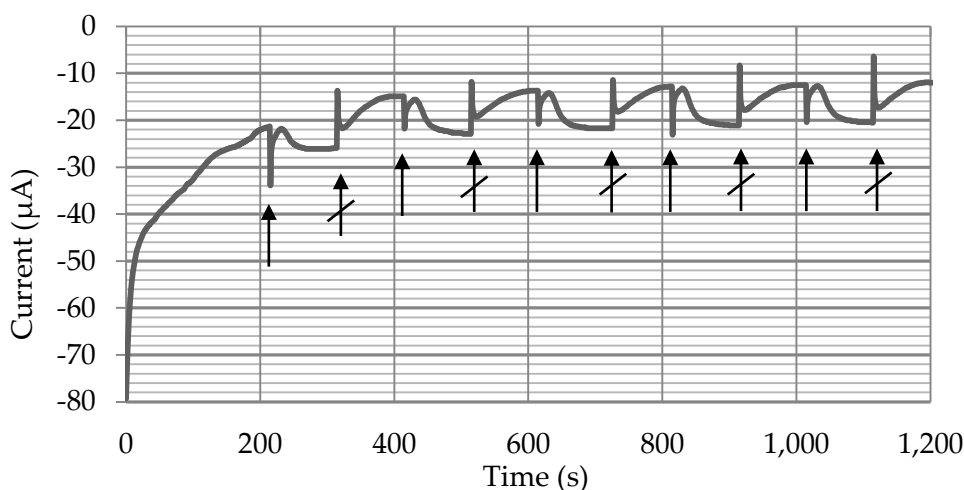


Figure 34: Chrono amperometric measurement of the 50% sample, measured at 0.2 V. At an open arrow the light is switched on and at a crossed arrow the light is turned off

The interesting value is the photocurrent: the difference between the observed current under illumination and in the dark. This photocurrent is found by plotting the average of the last few measurement points² before the light is either switched off or on. The absolute³ values of these points are plotted in Figure 35.

To find an accurate value for the photocurrent, a fit of these points is made, this fit is accurate for the measured values and does not predict values before or after the measured data. By subtracting the fit for the current in the dark ($I_{off}(t)$) from the current under illumination ($I_{on}(t)$), the photocurrent is found as a function of the time ($I_{ph}(t)$) as is shown in equation 9. Integrating this new equation over the measured time (400-1100 for Figure 35), and dividing this value by the measured time (700s for Figure 35) the average photocurrent (\bar{I}_{ph}) is found (eq. 10). Following this procedure led to a photocurrent of 8.62 μA , since the measured surface was a circle with a diameter of 6mm, the photocurrent density is 30.5 $\mu\text{A}/\text{cm}^2$.

$$I_{ph}(t) = |I_{on}(t) - I_{off}(t)| \quad 9$$

$$\bar{I}_{ph} = \int_{t_{start}}^{t_{end}} \frac{I_{ph}(t)}{t_{total}} dt \quad 10$$

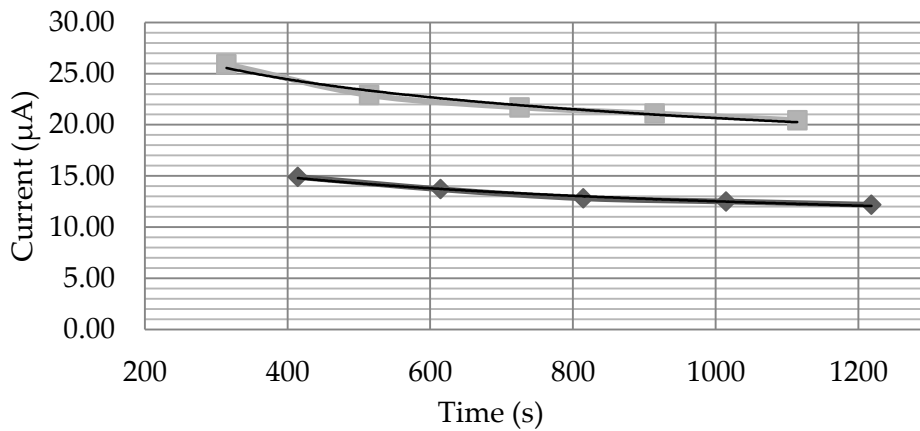


Figure 35: Plot of the absolute values of the current right before either switching on or off, for the 50% sample. The light curve shows the current under illumination, the dark line the current in the dark. The fit is shown as a black line.

For the 60% sample the measured data is shown below in Figure 36. Using the same procedure as for the 50% sample, shown in Figure 37, a photocurrent of 10.0 μA is found, resulting in a photocurrent density of 35.4 $\mu\text{A}/\text{cm}^2$, indeed an increase.

² For the 50% these are the last 5 points, for the 60% and 80% the last 100, due to different resolutions used for the measurements.

³ Since absolute values are plotted, it is noted that the illuminated current lies above the dark current.

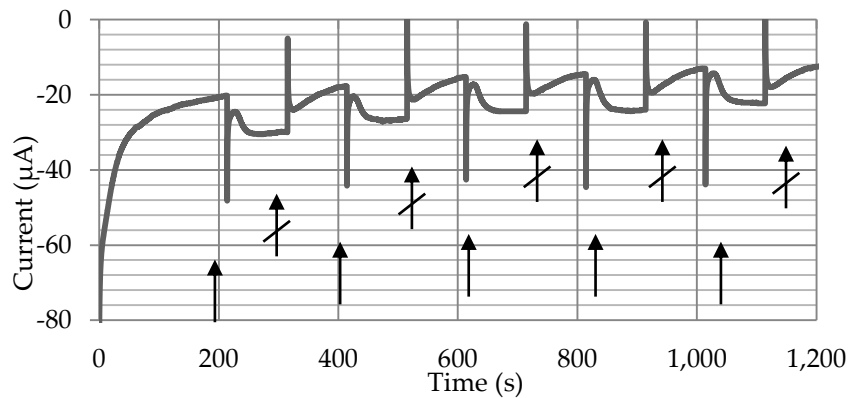


Figure 36: Chrono amperometric measurements of the 60% sample, measured at 0.2 V.

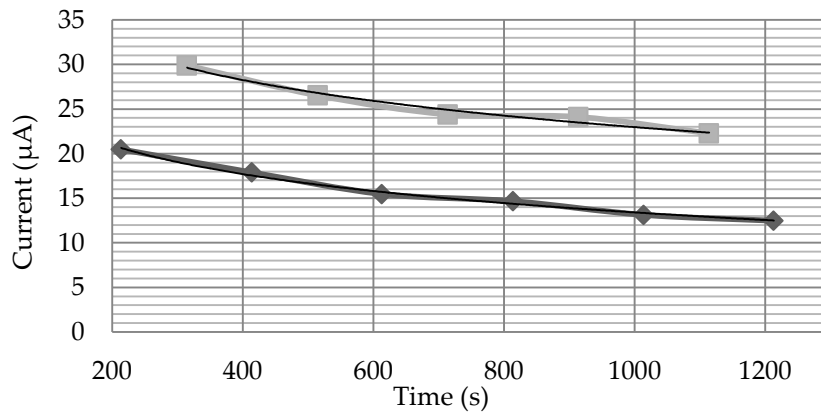


Figure 37: Plot of the absolute values of the current before either switched on or off, for the 60% sample. The light curve shows the current under illumination, the dark line the current in the dark. The fit is shown as a black line.

For the 80% sample the measured data is shown in Figure 38. Using the same procedure again, the two currents for illumination and dark are found as shown in Figure 39. The photocurrent of this sample was found to be $13.42 \mu\text{A}$, or a photocurrent density of $46.8 \mu\text{A}/\text{cm}^2$.

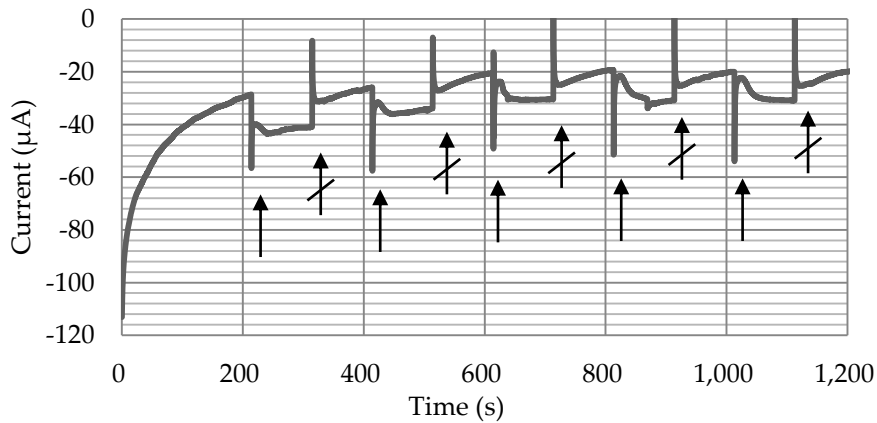


Figure 38: Amperometric measurement of the 80%, measured on 0.2 V.

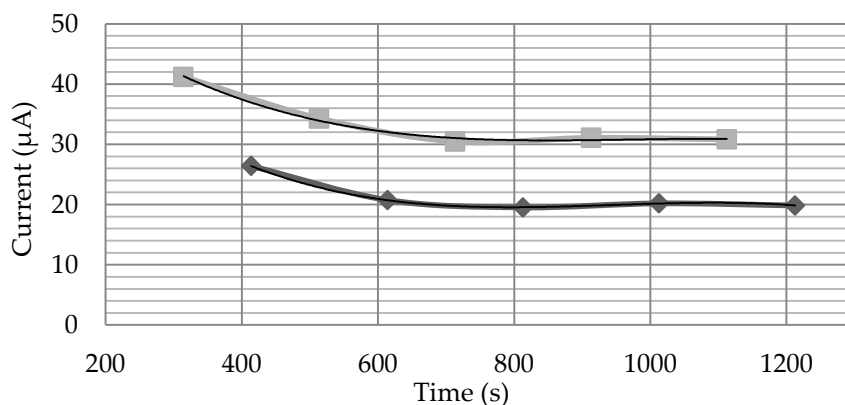


Figure 39: Plot of the absolute values of the current before either switched on or off, for the 60% sample. The light curve shows the current under illumination, the dark line the current in the dark. The fit is shown as a black line.

From these results we can conclude that the photocurrent is indeed generated by the nanowires, since the samples with fewer nanowires also had a lower current density. Important to mention is that the photocurrent depends on the length of the nanowires, since the broken wires (~20%, ~40% and ~50%) often leave a Cu_2O filled pore behind in the gold layer or a small stub. If the length of the nanowires wouldn't have had any effect on the photocurrent the difference in photocurrent would have been much smaller, since the broken wires take up the same surface as intact wires on the gold.

An electrodeposited thin layer of $1.5 \mu\text{m}$ p-type Cu_2O results in a photocurrent density of $\sim 40 \mu\text{A}/\text{cm}^2$ at 0.2V [37]. Our best sample gave a photocurrent density of $47 \mu\text{A}/\text{cm}^2$, which is already slightly higher, while only a small area of the surface is covered with nanowires. If it would be possible to deposit a bottom layer between the nano wires, the photocurrent will increase resulting in a significantly higher photocurrent compared to the thin layer Cu_2O .

4.2.2 Solar cell photocurrent

Also measurements on the solar cells were carried out. Five different samples were divided in four cells, giving a total of 20 cells to be measured. For each cell, an LSV measurement was carried out under illumination and in the dark. Of the 20 measured cells, 18 showed a more or less linear curve, with a rather high current ($\sim 0.1 \text{ A}$) this is a sign of short circuit since it behaves like a normal resistor. An example of this behaviour is shown in Figure 40.

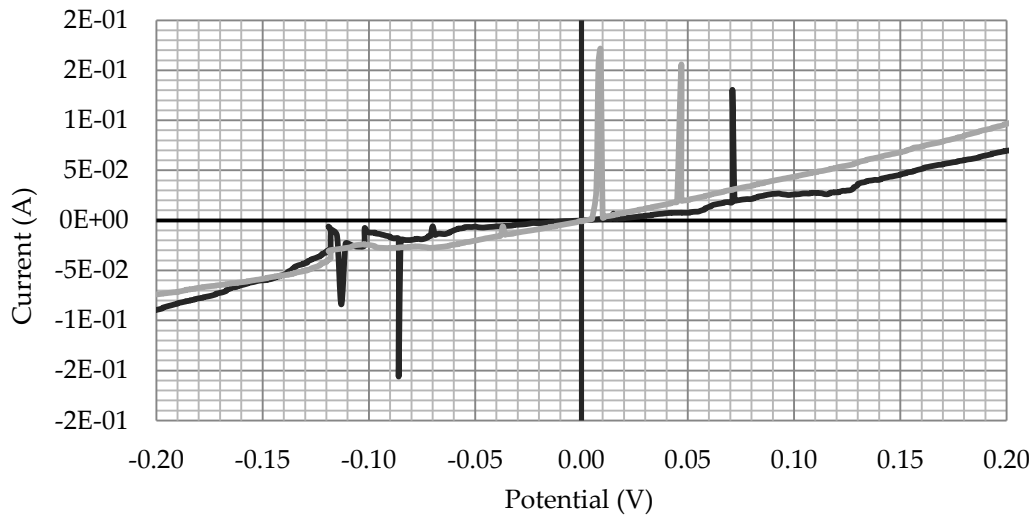


Figure 40: LSV measurement of a cell with an internal short circuit, the dark line is in the dark and the light line under illumination.

The other two cells, on two different samples, showed behaviour that is expected for a p-n diode. From now on these samples are called sample 1 and sample 2. The results of the LSV measurement of sample 1 are displayed in Figure 41a. The current in the dark shows the expected behaviour of a p-n diode; the current is negligible small for positive voltages, while for negative potentials a current is observed.

When the cell is illuminated again a p-n diode curve is observed. However it is less consistent compared to the curve in the dark. The curve is shifted, as is expected due to the photocurrent. However the direction of the shift is in contradiction to the theory in section 2.1.3, this is due to the fact that the electrodes were connected opposite.

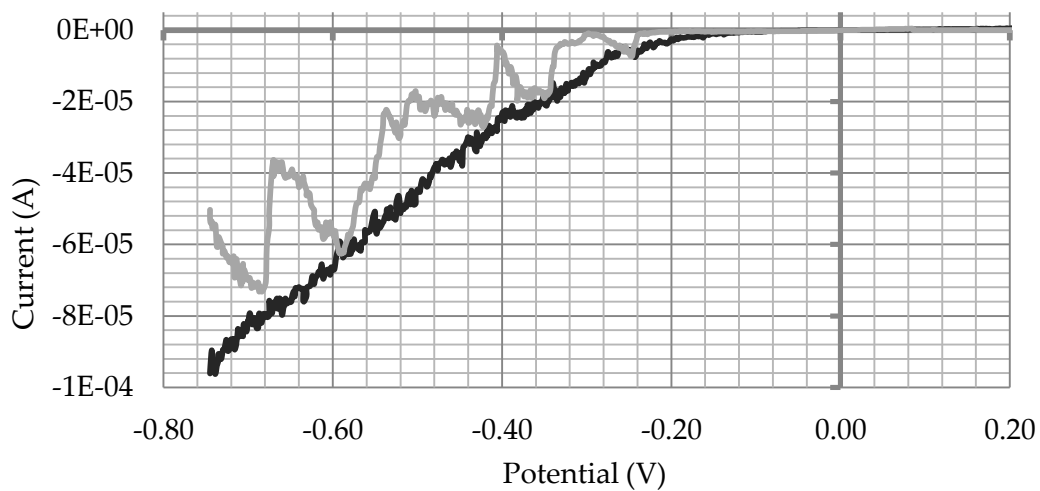


Figure 41a: LSV measurement, of sample 1, black curve is in the dark, light curve is under illumination.

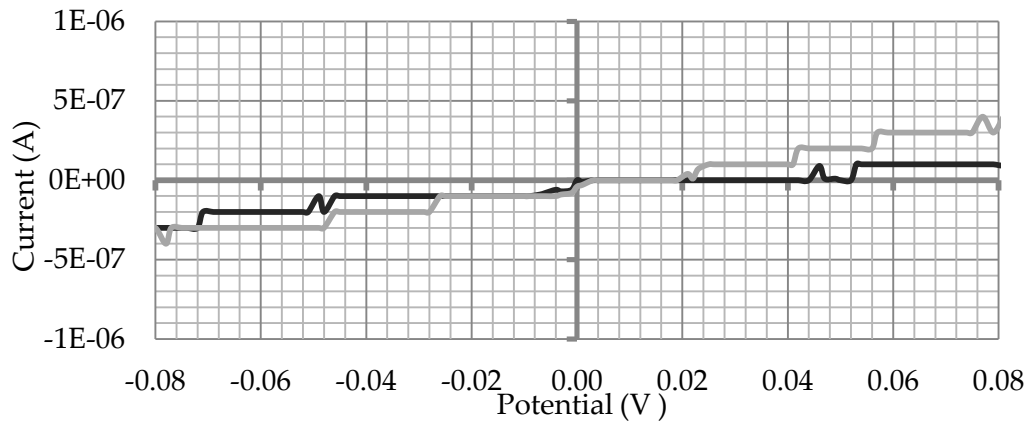


Figure 41b: Zoom of the LSV measurement above.

To get a definitive answer on the question if the sample is behaving as a solar cell, a zoom at the origin was made, shown in Figure 41b. If the sample would be behaving as a solar cell, the current curve under illumination should cross the y-axis at a positive value (short circuit current) and the x-axis at a negative value (open circuit potential). Unfortunately, the curve goes straight through the origin, so no photo generated current is present, and thus is this sample not a working solar cell.

For the second sample that showed p-n diode behaviour, the LSV measurements are shown in Figure 42. Strange behaviour was measured, on this sample, since the dark current was shifted around the origin instead of the illumination current. To rule out a measurement error, a second LSV measurement was performed in the dark on this sample which gave the same results. According to the measurements the solar cell even delivered a power in the dark, but under illumination the current crossed the origin so no power output was present. Where this strange behaviour originates from is unknown.

For more negative potentials the sample behaves as expected; the illuminated current is significantly less negative than the dark current. If only the origin would have been a little more to the left and down a working solar cell would have been created.

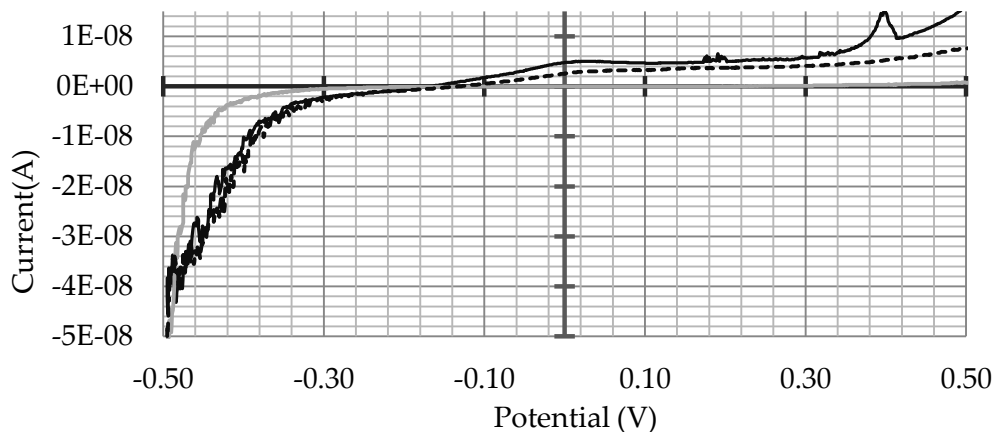


Figure 42: LSV measurement of sample 2, light is under illumination, dark is the first measurement in the dark and the dashed line is the second measurement in the dark.

5 Conclusions

The preparation route and characteristics of p-n homojunction Cu_2O nanowire solar cells were studied. In this chapter, the main results are summarised.

5.1 Preparation

Experiments showed that templated electrodeposition is an easy method for p-type Cu_2O nanowires synthesis. However, dissolution of the template was found to be challenging and improvements have been made on this aspect. In an environment with increased temperature of the solvent, a significant increase in the degree of dissolved template was found. However a layer of ~40nm of polycarbonate was still present and no method was found to dissolve this residual layer. The nanowires standing on the substrate have found to be very fragile, so introducing a small amount of flow breaks the nanowires. Therefore flow is not an option to dissolve the residual polycarbonate.

Deposition of the bottom layer of p-type Cu_2O was not successful due to the residual polycarbonate. Instead of deposition on the bottom, the p-type Cu_2O was deposited on top of the nanowires, which lead to nanowires with a cubic crystal on top of them. After this deposition an organic layer was found of which the origins are still unknown. Since it is an organic, it probably originates from the glue of the different tapes used.

The results of the unsuccessful p-type Cu_2O bottom deposition in combination with the found residual polycarbonate layer lead to a different preparation method. In this method, the n-type Cu_2O is deposited directly on top of the nanowires without any bottom layer of p-type Cu_2O , since the residual polycarbonate layer acts as insulation between the gold back contact and n-type Cu_2O .

By a sequence of pulses it was possible to deposit a rather homogenous layer on top of the nanowires. However these kind of samples will always contain some local regions with no or very few nanowires, where it is not possible to deposit a continuous layer on top of the nanowires. The deposition of the top layer can cause a short circuit if the polycarbonate layer is not sufficiently thick in these regions.

5.2 Characterization

Characterisation was done on both the nanowires and on the solar cells created by the alternative preparation method.

For the nanowires, chrono amperometric measurements were performed for measuring the photocurrent. These measurements showed clear p-type behaviour for the nanowires. The value of the found photocurrent density was slightly higher than measured previously for a thin layer of Cu_2O , 47 vs. 40 $\mu\text{A}/\text{cm}^2$. Considering that only a small surface area of the gold substrate is covered with the nanowires, this value could potentially increase even more for nanowire samples with a higher surface area.

For the prepared solar cells, linear sweep voltage measurements were performed. From the 20 cells that were prepared only 2 cells showed more or less p-n diode behaviour. However, the behaviour under illumination was not as expected and these 2 cells did not generate any photogenerated current, concluding that no working solar cells have been prepared. The other 18 samples showed a linear I-V curve, this is a sign that a simple resistor is measured. This is probably due to an internal short circuit.

6 Recommendations

The current preparation method has proven to be insufficient in creating a working solar cell. Future research should focus on either dissolving the membrane to a higher degree or a different preparation method.

In this thesis, one different preparation route compared to the initially proposed method has been tested, but this gave no satisfying results. Improvements on this route could be made by decreasing the dissolution time, which increases the thickness of the residual polycarbonate layer. Another idea is synthesising a membrane made of two parts of which one part is not soluble.

A different preparation route could be to increase the electrodeposition time to such a degree that Cu_2O is deposited on top of the membrane, creating a thin layer on the membrane. By using this top layer as the previously required bottom layer of p-type Cu_2O , the bottom deposition does not need to be carried out. With the use of gold etchant the gold back contact can be dissolved. By adhering this sample upside down to a glass substrate, the membrane can be dissolved leaving free standing wires with a p-type Cu_2O bottom. The use of a thinner membrane would be required, since the wires do not possess the structural strength to stay intact for a length longer than $1\ \mu\text{m}$.

A different method to skip the bottom deposition step, is to use Cu_2O (either n- or p-type) as a back electrode on the membrane. Results in this research showed that deposition is easily possible on Cu_2O . However the deposition of Cu_2O on the membrane will be challenging, since Cu_2O thin layer have been prepared using PLD [38], however the temperature ($500\ \text{°C}$) needed for this deposition would melt the PC membrane. With the use of a different membrane, that could endure this temperature, this method can be promising.

In the bottom deposition step, an organic layer was found, probably originating from the different tapes used. A method should be developed without the use of any tape to check if this statement is true and if this layer has any influence on the deposition. For instance by adhering the sample exactly on silver paste, on such a way that no silver paste is left uncovered.

Increasing the structural strength of the wires can also be beneficial since this opens the possibility to use flow in the solvent. This could be done by synthesising nanocones or thicker wires.

Decreasing the nanowire density can also lead to less residual polycarbonate on the gold and is worth to investigate.

Increasing the p-n junction interface can also be achieved by different methods than templated electrodeposition and are certainly worth investigation, i.e. with preferential absorption crystal structures can be electrodeposited without the use of any template. McShane et. al. have proven that an increased surface can be achieved with electrodeposition of dendritic n-type Cu_2O crystals without the use of any template [23].

Acknowledgements

This Bachelor's thesis wouldn't have been possible without the support of certain people. Therefore I would like to end this thesis by thanking them.

First of all I would like to thank my daily supervisor, Wouter Maijenburg, for the tremendous efforts he has made in the guidance of my research. I am thankful for all of the discussions we had about the challenges and results encountered in the research. Without his insights and knowledge, this research would not have achieved the level it did. The informal contact made it a pleasure to work together and in the same office and reduced the barrier for questions.

I thank André ten Elshof for giving me the opportunity to fulfil my research within the Inorganic Materials Science group. His feedback at the mid-term presentation and his reassuring words boosted my motivation for the second part of the research.

Special thanks go to Moreno de Respinis for putting the solar simulator setup of the TU Delft to our disposal, and his guidance during the measurements on the prepared samples. Without this setup it wouldn't have been possible to draw the conclusions about the photocurrent in this thesis. I also would like to thank him for pointing us to the sports bar at the TU Delft, which delivered great food for a perfect price.

I thank Frank Roesthuis for his clear explanation on the operation of the JEOL 6490 SEM. This made fast operation of the SEM possible, greatly increasing the amount of inspection possible on the samples. Without this possibility the amount of research would have been significantly less. He is also thanked for his explanation on the Perkin-Elmer 2400, increasing the number of samples prepared.

I thank Mark Smithers for his operation of the LEO 1550 SEM, this made it possible to achieve more detailed pictures, increasing the knowledge of the samples.

I thank Mark Huijben for his feedback during the mid-term presentation. His knowledge on materials for energy conversion greatly helped me to put this research in the bigger picture.

I thank Jaap Flokstra for his outsider view on this research. Unfortunately he could not take seat in the bachelor committee till the end.

I thank Herman Hemmes for his replacement of Jaap Flokstra on such a short notice. Without his replacement I wouldn't be possible to finish my bachelor's assignment this academic year.

I thank Maarten Nijland for his assistance in the pulsed laser deposition of the top electrode. This wouldn't have been possible without the settings Matthijn Dekkers supplied me with, for which I would like to thank him.

I thank Victor Schouten for his point of view on the many experiments we did together, and his idea to use a static electrical charged plastic sheet for the preparation of the samples, which greatly increased the preparation speed.

I thank Rogier Besselink for his vast knowledge on a broad spectrum of topics, his feedback on my work and being my office partner for the time of the assignment.

As last I would like to mention the great atmosphere in the IMS group. It has always been great to work in this group, which went hand in hand with informal contact between the other members of IMS. The Wednesday colloquia were interesting, good to get to know people inside the group, and kebab, pizza and Chinese food are a great lunch to start a productive afternoon.

References

1. Borgstrom, M., et al., *Nanowires with promise for photovoltaics*. Selected Topics in Quantum Electronics, IEEE Journal of, 2010(99): p. 1-12.
2. Rai, B., *Cu₂O solar cells: A review*. Solar Cells, 1988. **25**(3): p. 265-272.
3. McShane, C.M., et. al., *Effect of junction morphology on the performance of polycrystalline Cu₂O homojunction solar cells*. The Journal of Physical Chemistry Letters, 2010. **1**: p. 2666-2670.
4. Maas, M.G., et al., *Microstructure development in zinc oxide nanowires and iron oxhydroxide nanotubes by cathodic electrodeposition in nanopores*. Journal of Materials Research, 2011. **1**(1): p. 1-7.
5. Rodijk, E., et al., *Templated electrodeposition of Ag₇NO₁₁ nanowires with very high oxidation states of silver*. Materials Letters, 2011.
6. Maas, M.G., et al. *Photocatalytic Segmented Nanowires and Single-step Iron Oxide Nanotube Synthesis: Templated Electrodeposition as all-round Tool*. 2009. Cambridge Univ Press.
7. Maijenburg, A.W., et al., *Dielectrophoretic alignment of metal and metal oxide nanowires and nanotubes: a universal set of parameters for bridging prepatterned microelectrodes*. J Colloid Interface Sci, 2011. **355**(2): p. 486-93.
8. Maijenburg, A.W., et al., *Hydrogen generation from photocatalytic silver/zinc oxide nanowires: towards multifunctional multisegmented nanowire devices*. Small, 2011. **7**(19): p. 2709-13.
9. Mills, D., *Advances in solar thermal electricity technology*. Solar Energy, 2004. **76**(1): p. 19-31.
10. Schaffer, J.P., et al., *The science and design of engineering materials*1995: Irwin.
11. Kittel, C. and P. McEuen, *Introduction to solid state physics*. Vol. 7. 1976: Wiley New York.
12. Tipler, P.A, et. al., *Physics for scientists and engineers*. Vol. 1. 2008: Macmillan.
13. Atkins, P. and J. de Paula, *Atkins' physical chemistry*. Chemistry, 2006.
14. Lorenzo, E., *Solar electricity: engineering of photovoltaic systems*1994: James & James Science Publishers.
15. Luque, A., et. al., *Handbook of photovoltaic science and engineering*2010: Wiley.
16. Zeman, M., *Solar Cells - Operation principles*. 2008: p. 4.1-4.26
17. WATSON, G.W., *Modeling the polaronic nature of p-type defects in Cu₂O: The failure of GGA and GGA plus U*. 2009.
18. Malerba, C., et al., *Absorption coefficient of bulk and thin film Cu₂O*. Solar Energy Materials and Solar Cells, 2011.
19. De Jongh, P., et. al., *Cu₂O: electrodeposition and characterization*. Chemistry of materials, 1999. **11**(12): p. 3512-3517.
20. Wang, L., et. al. *Fabrication and Characterization of p-n Homojunctions in Cuprous Oxide by Electrochemical Deposition*. Electrochemical and Solid-State Letters, 2007. **10**(9): p. H248.
21. Fernando, C.A.N., et al., *Investigation of n-type Cu₂O layers prepared by a low cost chemical method for use in photo-voltaic thin film solar cells*. Renewable Energy, 2002. **26**(4): p. 521-529.

22. McShane, C.M., et. al., *Junction studies on electrochemically fabricated p-n Cu₂O homojunction solar cells for efficiency enhancement*. *Phys Chem Chem Phys*, 2012. **14**(17): p. 6112-8.
23. McShane, C.M., et. al., *Photocurrent Enhancement of n-Type Cu₂O Electrodes Achieved by Controlling Dendritic Branching Growth*. *Journal of the American Chemical Society*, 2009. **131**(7): p. 2561-2569.
24. Tan, B., et. al., *Dye-sensitized solar cells based on anatase TiO₂ nanoparticle/nanowire composites*. *The Journal of Physical Chemistry B*, 2006. **110**(32): p. 15932-15938.
25. Nakade, S., et al., *Influence of TiO₂ nanoparticle size on electron diffusion and recombination in dye-sensitized TiO₂ solar cells*. *The Journal of Physical Chemistry B*, 2003. **107**(33): p. 8607-8611.
26. Choi, K.S., *Shape control of inorganic materials via electrodeposition*. *Dalton Trans*, 2008(40): p. 5432-8.
27. Weickert, J., et al., *Nanostructured organic and hybrid solar cells*. *Adv Mater*, 2011. **23**(16): p. 1810-28.
28. Kislyuk, V.V., et. al., *Nanorods and Nanotubes for Solar Cells*. *Journal of Nanoscience and Nanotechnology*, 2008. **8**(1): p. 131-148.
29. Rakhshani, A., *Preparation, characteristics and photovoltaic properties of cuprous oxide—a review*. *Solid-state electronics*, 1986. **29**(1): p. 7-17.
30. Nolan, M., et. al., *The p-type conduction mechanism in Cu₂O: a first principles study*. *Phys. Chem. Chem. Phys.*, 2006. **8**(45): p. 5350-5358.
31. Siripala, W., et. al., *Observation of n-type photoconductivity in electrodeposited copper oxide film electrodes in a photoelectrochemical cell*. *Solar energy materials*, 1986. **14**(1): p. 23-27.
32. Garuthara, R., et. al., *Photoluminescence characterization of polycrystalline n-type Cu₂O films*. *Journal of Luminescence*, 2006. **121**(1): p. 173-178.
33. Xiong, L., et al., *p-Type and n-type Cu₂O semiconductor thin films: Controllable preparation by simple solvothermal method and photoelectrochemical properties*. *Electrochimica Acta*, 2011. **56**(6): p. 2735-2739.
34. Meyyappan, M., et. al., *Inorganic nanowires* 2010: CRC Press.
35. Bard, A.J., et. al., *Electrochemical methods: fundamentals and applications*. Vol. 2. 1980: Wiley New York.
36. Choi, K.S., et al., *Electrochemical synthesis of inorganic polycrystalline electrodes with controlled architectures*. *MRS bulletin*, 2010. **35**(10): p. 753-760.
37. Somasundaram, S., et al., *Photocatalytic production of hydrogen from electrodeposited p-Cu₂O film and sacrificial electron donors*. *International Journal of Hydrogen Energy*, 2007. **32**(18): p. 4661-4669.
38. Chen, A., et al., *Controlled growth and characteristics of single-phase Cu₂O and CuO films by pulsed laser deposition*. *Vacuum*, 2009. **83**(6): p. 927-930.